CENTER FOR INFRASTRUCTURE ENGINEERING STUDIES

Micro-Macro Modeling of the External Strengthening of

Concrete with Fiber Reinforced Polymer: Phase I, II, & III

By

Dr. Samit Roy

Dr. Lokeswarappa R. Dharani

Technical Report Documentation Page

1. Report No. UTC R41-R57-R77A	2. Government Accession No.	3. Recipient's Catalog No.
4. Title and Subtitle Micro-Macro Modeling of the External Strengthening of Concrete with Fiber Reinforced Polymer: Phase I, II, & III		5. Report Date Dec 2002
		6. Performing Organization Code
7. Author/s Dr. Samit Roy, Dr. Lokeswarappa R. Dharani		8. Performing Organization Report No. RG000922
9. Performing Organization Name and Address Center for Infrastructure Engineering Studies/UTC program University of Missouri - Rolla 223 Engineering Research Lab Rolla, MO 65409		10. Work Unit No. (TRAIS)
		11. Contract or Grant No. DTRS98-G-0021
12. Sponsoring Organization Name and Address U.S. Department of Transportation Research and Special Programs Administration 400 7th Street, SW Washington, DC 20590-0001		13. Type of Report and Period Covered Final
		14. Sponsoring Agency Code
15. Supplementary Notes		
16. Abstract A large number of bridges in the federal inventory are reaching the end of their design life due to aging and environmental degradation. The situation is aggravated by increased traffic needs that require existing structures to carry heavier loads at increasingly higher speeds.		

16. Abstract

A large number of bridges in the federal inventory are reaching the end of their design life due to aging and environmental degradation. The situation is aggravated by increased traffic needs that require existing structures to carry heavier loads at increasingly higher speeds.

17. Key Words Retrofitting, flexural members and load capacity	18. Distribution Statement No restrictions. This document is available to the public through the National Technical Information Service, Springfield, Virginia 22161.		
19. Security Classification (of this report) unclassified	20. Security Classification (of this page) unclassified	21. No. Of Pages	22. Price

Form DOT F 1700.7 (8-72)

FINAL REPORT
July 2004

UTC Project:
Micro-Macro Modeling of the External Strengthening of Concrete with Fiber Reinforced Polymer

Faculty: Samit Roy and Lokeswarappa R. Dharani

Graduate Students: Ravi Karedla and Jun Wei

Project Summary:
The issue of moisture diffusion in composite materials is important because of its associated problem of freeze and thaw. The volumetric expansion of water when it freezes to form ice results in stress concentrations at the inclusion tip that may synergistically interact with the residual tensile stresses in a laminate at low temperatures to initiate a crack. In addition, understanding the long-term effect of daily and/or seasonal freeze-thaw cycling on crack growth is of vital importance for structural durability.

A theoretical framework for the calculation of the stress intensity factor, K_I, of a pre-existing crack in a composite structure due to the phase transition of trapped moisture. The constrained volume expansion of trapped moisture is postulated to be the crack driving force. The principle of minimum strain energy is employed to calculate the elastic field within an orthotropic laminate containing an idealized elliptic inclusion in the form of ice. It is postulated that a slender elliptical inclusion can be used to approximate the stress field at the crack face, which can be used to calculate the stress intensity factor for the crack.

The model developed as above, is verified. The verification is based on comparisons of the stresses in an elliptic elastic inclusion and the stress intensity factor with a special isotropy and with finite element analysis for the case of orthotropy. The results indicate that the stress state in a slender elliptic elastic inclusion can be used to approximate the stress field at the crack tip, which could subsequently be adopted to determine the stress intensity factor. Analyses of the delamination and fatigue life prediction for freeze-thaw cycling are provided as specific applications of the model.

UTC Project:
Micro-Macro Modeling of the External Strengthening of Concrete with Fiber Reinforced Polymer

Publications:

Roy R., Nie, G. H., Karedla, R. and L. R. Dharani, " Matrix Cracking and Delaminations in Orthotropic Laminates Subjected to Freeze-Thaw: Model Development", Polymers and Polymer Composites, Vol. 10, No. 5, 2002, pp. 327-34.

Roy R., Nie, G. H., Karedla, R. and L. R. Dharani," Stress Intensity Factor for an Elliptic Inclusion in Orthotropic Laminates Subjected to Freeze-Thaw: Model Verification", Polymers and Polymer Composites, Vol. 10, No. 9, 2002, pp. 571-588.

Matrix Cracking and Delaminations in Orthotropic Laminates Subjected to Freeze-Thaw: Model Development

Samit Roy*, G.H. Nie*, R. Karedla** and L. Dharani**

*Mechanical and Aerospace Engineering Department, Oklahoma State University
**Mechanical and Aerospace Engineering Department, University of Missouri-Rolla

SUMMARY

With the increasing use of fibre composites in applications such as cryogenic liquid hydrogen tanks and repair/retrofitting of bridges, the diffusion and freezing of moisture to form ice is an issue of growing importance. The volumetric expansion of water when it freezes to form ice results in stress concentrations at the inclusion tip that may synergistically interact with the residual tensile stresses in a laminate at low temperatures to initiate a crack. In addition, understanding the long-term effect of daily and/or seasonal freeze-thaw cycling on crack growth in a laminate is of vital importance for structural durability.

The objective of this paper is to establish a theoretical framework for the calculation of the stress intensity factor (K_I) of a pre-existing crack in a composite structure due to the phase transition of trapped moisture. The constrained volume expansion of trapped moisture due to freezing is postulated to be the crack driving force. The principle of minimum strain energy is employed to calculate the elastic field within an orthotropic laminate containing an idealized elliptical elastic inclusion in the form of ice. It is postulated that a slender elliptical elastic inclusion can be used to approximate the stress field at the crack face, which can subsequently be used to calculate the stress intensity factor, K_I, for the crack. The verification of the analytical model predictions and some potential applications will be published in a separate paper.

1. INTRODUCTION

The use of fibre reinforced polymers (FRP) for infrastructure retrofit has experienced widespread use in Western Europe and Japan, but has only recently been attempted in the United States. Despite the fact that FRP composites have seen extensive application as performance enhancing materials in the aerospace and defence industries, their application in the civil engineering sector has been slow. One of the chief reasons is a lack of reliable predictive models and sound design guidelines for their use in civil infrastructure applications, especially in aggressive environments that involve extreme temperatures and humidity.

These FRP laminates may contain flaws such as matrix cracks and voids as a result of the manufacturing processes. These flaws result in stress concentrations that, in conjunction with internal residual stresses, may lead to initiation of larger cracks. When these cracks are filled with a material, then we have something called an 'inclusion problem'. These inclusions disturb the uniformity of an elastic medium because the inclusion has elastic properties differing from those of the surrounding matrix.

One example of an inclusion problem is the freezing of moisture in pre-existing cracks in FRP and in FRP bonded interfaces. With the increasing use of fibre composites in application such as cryogenic liquid hydrogen tanks and repair/retrofitting of bridges etc., the diffusion and freezing of moisture to form ice is an issue of growing importance. The volumetric expansion of water when it freezes to form ice results in stress concentrations at the inclusion tip that may synergistically interact with the residual tensile stresses in a laminate at low temperatures to initiate a crack. In addition, understanding the long-term effect of daily and/or seasonal freeze-thaw cycling on crack growth in a laminate is of vital importance for structural durability.

Most of the studies in the theory of elasticity have focused primarily on structures with inclusions with far field-applied stress. Some of these studies investigated martensitic transformation (thermal expansion, phase transition or plastic flow), but have limited themselves to the calculation of stresses in the inclusion-matrix system, with no discussion of crack growth.

Verghese at al[1] showed by presenting data obtained from differential scanning caloriemetry (DSC) that a composite system did have traces of freezable water. Scanning electron and optical micrographs shown by the authors indicate the presence of interfacial cracks in composites. DSC data on a neat, unreinforced vinyl ester resin sample showed no freezable water. Though water resides in the free volume in a polymer, the space available is too small to allow water to freeze from a thermodynamic perspective. However, experiments on a glass vinyl ester composite showed interfacial cracks large enough for water to freeze. Verghese et. al. conclude that it is impossible to freeze water in a pure resin, like vinyl ester. However, composite systems have crack dimensions large enough to facilitate the freezing of water.

Lord and Dutta[2] highlighted the importance of cracks in the matrix and fibre-matrix interface as being the cause of the damage in composite materials. When these cracks form beyond a certain critical size and density they grow to form macroscopic matrix cracks. They also focused attention on thermally induced residual stresses. Decreasing the temperature from the cure temperature to room or cold temperatures produces residual stresses, due to the difference between fibre and matrix stiffness for a single layer unidirectional lamina. In the case of a multilayered laminate, residual stress are produced when the laminate is subjected to a change in temperature because of differences between the elastic properties in adjacent plies. The authors showed that these residual stresses are of significant magnitude and can lead to the creation of microcracks. Moreover, when the moisture condensate freezes, internal stresses are caused in the laminate that could initiate crack propagation and/or ply delamination.

Dutta[3] also carried out experiments on the effect of cold temperature thermal cycling on the stiffness properties on a number of composites. He noted that there was little effect on fibre-dominated behaviour such as tensile and flexural stiffness. On the other hand, significant reduction was observed in the matrix dominated torsional stiffness as a result of low temperature thermal cycling. Acoustic emission results showed increased rate of acoustic emissions at decreasing temperatures, which indicates the development of micro cracks.

The determination of the effects of holes and cavities, or flaws, in an elastic solid when the stress at points remote from the flaw is uniform has been achieved for circular and elliptical holes. Goodier[4] applied solutions of elasticity to investigate the effect of small spherical and cylindrical inclusions. He derived numerical results for gaseous inclusions, perfectly rigid inclusions and slag globules in steel and reinforcing rods in concrete.

Donnell[5] found the stress distribution for the case of an infinite plate under any uniform direct or shear edge forces, having an elliptical hole (or region) filled with a material of different stiffness from the rest of the plate. The stiffness ratio between the moduli of elasticity of the inclusion and the matrix was allowed to have any value, but the Poisson's ratio was assumed to be the same for both the inclusion and the matrix. Also, the solution was strictly two-dimensional.

Eshelby[6] considered martensitic transformation for an ellipsoid. The inclusion in a homogeneous elastic medium undergoes a permanent change of form, which, in the absence of the constraint imposed by the surrounding (the matrix), would be a prescribed uniform strain. Because of the displacement constraint on the inclusion due to the presence of the matrix, stresses will be present in both the inclusion and the matrix. The elastic field was found with the help of a sequence of imaginary cuttings, straining and welding operations. The strain in the ellipsoid was expressed in the form of elliptical integrals and it was found to be uniform.

The three-dimensional inhomogeneity problem was also discussed by Eshelby[7]. Special cases of inclusions and inhomgeneities in the form of the general ellipsoid with three unequal axes were considered. Formation of precipitates was also given consideration in this analysis.

Although Eshelby has demonstrated some general theorems of great interest for martensitic transformation using elegant methods, his solutions involved analytically intractable integrals of a formidable nature. This applies even in two-dimensional situations, i.e. where the inclusion has the shape of a long cylinder of elliptical cross-section,

under conditions of plane strain or appears as an elliptical region of a thin plate under conditions of generalized plane stress. Jaswon and Bhargava[8] obtained explicit solutions in these cases by an approach based on complex variable formulation. A detailed quantitative analysis of the stress and displacement in the surrounding matrix outside the elliptical inclusion thus becomes possible.

Bhargava and Radhakrishna[9] studied the above martensitic transformation problem using the minimum strain potential method. They determined the elastic field in the infinite medium (the matrix) around the inclusion, the strain energy and the equilibrium size of an elliptical inclusion, with elastic constants differing from those of the matrix.

The elastic field generated in two bonded isotropic half-planes containing either a circular or a rectangular inclusion was solved by Aderogba and Berry[10]. The analysis was based upon the two-dimensional form of the Papkovich-Neuber stress function approach.

Stress state and crack extension criteria for a two-dimensional elastic problem of a crack lying along the interface of a rigid circular inclusion embedded in an infinite elastic solid have been considered by Toya[11]. He assumed that the interfacial crack is opened by equal and opposite normal pressures on opposite sides of the crack. The formulation presented by Muskhelishvili[12] was used for the explicit solution of stresses and displacements. The stresses and displacements solutions were then applied in conjunction with Griffith's virtual work argument to solve the conditions for which the crack growth may occur along the interface.

A crack lying along the interface of an elastic circular inclusion, embedded in an infinite elastic solid, was also considered by Toya[13]. It was assumed that each of the two materials was homogeneous and isotropic. The stress state at infinity is general biaxial tension and the crack faces were free from traction, unlike in Toya's previous work[11].

Motivation for the present study originates from the fact that composite materials are being used increasingly in low temperature environments. The existence of interfacial cracks and the freezability of moisture in voids has been clearly established by researchers[1,2,3]. A review of the literature shows that although extensive work has been done on stress fields in structures with inclusions[4,6,9], a framework

for the analysis of freeze-thaw in orthotropic composite structures based on fracture mechanics is yet to be established. In addition, a guideline for the conditions of crack growth in composites due to daily and/or seasonal freeze-thaw cycles is necessary for safe structural design.

The objective of this work is to establish a theoretical framework for the calculation of the stress intensity factor (K_I) of a pre-existing crack in a composite structure due to the phase transition of trapped moisture. The constrained volume expansion of trapped moisture due to freezing is postulated to be the crack driving force. The principle of minimum strain energy is employed to calculate the elastic field within an orthotropic laminate containing an idealized elliptical elastic inclusion in the form of ice. It is postulated that a slender elliptical elastic inclusion can be used to approximate the stress field at the crack face, which can subsequently be used to calculate the stress intensity factor, K_I, for the crack. The verification of the analytical model predictions and some model applications will be presented in a separate paper.

2. MODELING OF STRESSES DUE TO AN ELLIPTICAL INCLUSION IN AN ORTHOTROPIC MEDIUM

In this section it is postulated that the problem of an ice filled cavity in FRP is equivalent to that of an inclusion problem. An inclusion, which undergoes volumetric dilatation due to temperature change and/or phase change, can be replaced by an equivalent traction force acting on the interface between the matrix and the inclusion. The schematic shown in **Figure 1** depicts the equivalence.

The theory of minimum strain energy was used to model the inclusion in an orthotropic medium. The theory[14] states that the displacement field that satisfies the differential equations of equilibrium, as well as the conditions at the bounding surface, yields a smaller value for the potential energy of deformation than any other displacement field that satisfies the same configurations at the bounding surface.

Following the strain-energy method for isotropic material presented by Bhargava and Radhakrishna[9], the present approach consists of taking an arbitrarily fixed position of the common boundary of inclusion and matrix, and considering the resulting equilibrium configuration. It should be noted that in this

Samit Roy, G.H. Nie, R. Karedla and L. Dharani

Figure 1 Inclusion problem equivalence assumption
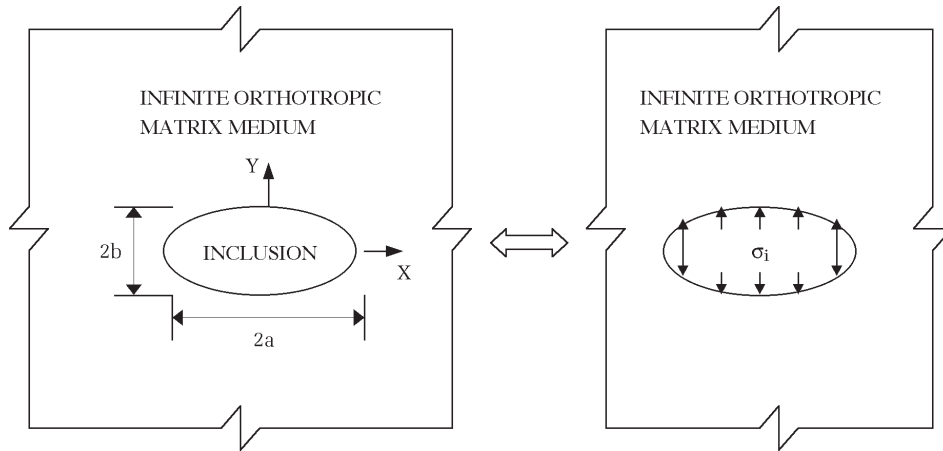
derivation, both the inclusion and the surrounding matrix medium are assumed to be orthotropic elastic. The elastic displacements of the inclusion are calculated with reference to the free surface configuration. From these displacements, the elastic strain energy in the inclusion is then derived. The elastic displacement of the interior boundary of the matrix medium is calculated from the initial unperturbed position. Given the displacement of the interior of the matrix, the elastic stress and strain fields in the matrix can be calculated by the complex variable method. From these elastic fields, the elastic strain energy of the matrix is then obtained. The sum total of the energy in the inclusion-matrix system is a scalar addition of the individual strain energies. Finally, the equilibrium position is obtained by minimizing the total strain energy.

2.1 Stress-Strain Relations

The generalized Hooke's law gives the stress-strain relation for the orthotropic matrix and can be written in tensor notation as

$$\sigma_i = c_{ij}\varepsilon_j \tag{1}$$

conversely, $\varepsilon_j = a_{ij}\sigma_i \quad i,j = 1,...,6$

where e_i are the six strain components, s_j are the six stress components based on the Voigt notation, a_{ij} is the compliance matrix and c_{ij} is the stiffness matrix.

The stiffness matrix, c_{ij} consists of 36 constants. However, the stiffness matrix is symmetric, by strain energy consideration. Thus, not all 36 constants are independent. For a characteristic anisotropic material there are only 21 independent constants in the compliance matrix.

Further, if there are two orthogonal planes of material property symmetry for a material, symmetry will exist relative to a third mutually orthogonal plane. The stress-strain relation in coordinates aligned with principal material directions are said to define an orthotropic material and have only 9 independent constants. The stress strain relationship for orthotropic material is shown in Equation (2)[15].

If at every point of a material there is one plane in which the mechanical properties are equal in all directions, then the material is called transversely isotropic. For this case, $a_{22} = a_{11}, a_{23} = a_{13}, a_{55} = a_{44}$ and $a_{66} = 2(a_{11} - a_{12})$, the stress strain relations thus have only five independent constants.

If there are an infinite number of planes of material property symmetry, then the relation simplifies to the isotropic material relations with only two independent constants. Then the stress-stain relation in terms of compliance matrix is given as in Equation (3).

The engineering constants are generally the slope of a stress-strain curve (e.g., $E = \sigma/\varepsilon$) or the slope of a strain-strain curve (e.g. $v = -\varepsilon_y/\varepsilon_x$). Thus, the components of the compliance matrix, a_{ij}, are determined more directly than those of the stiffness matrix, c_{ij}. For an orthotropic material, the compliance matrix components in terms of the engineering constants are shown in Equation (4),

$$\begin{bmatrix} \varepsilon_x \\ \varepsilon_y \\ \varepsilon_z \\ \gamma_{yz} \\ \gamma_{zx} \\ \gamma_{xy} \end{bmatrix} = \begin{bmatrix} a_{11} & a_{12} & a_{13} & 0 & 0 & 0 \\ & a_{22} & a_{23} & 0 & 0 & 0 \\ & & a_{33} & 0 & 0 & 0 \\ symmetrical & & & a_{44} & 0 & 0 \\ & & & & a_{55} & 0 \\ & & & & & a_{66} \end{bmatrix} \begin{bmatrix} \sigma_x \\ \sigma_y \\ \sigma_z \\ \tau_{yz} \\ \tau_{zx} \\ \tau_{xy} \end{bmatrix} \tag{2}$$

$$\begin{bmatrix} \varepsilon_x \\ \varepsilon_y \\ \varepsilon_z \\ \gamma_{yz} \\ \gamma_{zx} \\ \gamma_{xy} \end{bmatrix} = \begin{bmatrix} a_{11} & a_{12} & a_{12} & 0 & 0 & 0 \\ & a_{11} & a_{12} & 0 & 0 & 0 \\ & & a_{11} & 0 & 0 & 0 \\ symmetrical & & 2(a_{11}-a_{12}) & 0 & 0 \\ & & & 2(a_{11}-a_{12}) & 0 \\ & & & & 2(a_{11}-a_{12}) \end{bmatrix} \begin{bmatrix} \sigma_x \\ \sigma_y \\ \sigma_z \\ \tau_{yz} \\ \tau_{zx} \\ \tau_{xy} \end{bmatrix} \tag{3}$$

$$[a_{ij}] = \begin{bmatrix} \dfrac{1}{E_1} & \dfrac{-v_{12}}{E_1} & \dfrac{-v_{13}}{E_1} & 0 & 0 & 0 \\[2mm] & \dfrac{1}{E_2} & \dfrac{-v_{23}}{E_2} & 0 & 0 & 0 \\[2mm] & & \dfrac{1}{E_3} & 0 & 0 & 0 \\[2mm] symmetrical & & & \dfrac{1}{G_{23}} & 0 & 0 \\[2mm] & & & & \dfrac{1}{G_{31}} & 0 \\[2mm] & & & & & \dfrac{1}{G_{12}} \end{bmatrix} \tag{4}$$

where E_1, E_2, E_3 = Young's (extension) moduli in the x-, y- and z-directions; v_{ij} = Poisson's ratio ($v_{12} = -\varepsilon_y/\varepsilon_x$, $v_{13} = -\varepsilon_z/\varepsilon_x$, $v_{23} = -\varepsilon_z/\varepsilon_y$); G_{23}, G_{31}, G_{12} = shear moduli in the y-z, z-x and x-y planes.

Equation (4) reduces to the compliance matrix for an isotropic material by substituting $E_1 = E_2 = E_3 = E$, $G_{23} = G_{31} = G_{12} = G$ and $v_{ij} = v$.

The three principal direction x, y and z are as shown in **Figure 2**.

Under plane strain conditions we have $\varepsilon_z = 0$. Thus, eliminating σ_z from Equation (2), the stress-strain relation reduces to Equation (5).

Figure 2 Principal directions of an orthotropic material
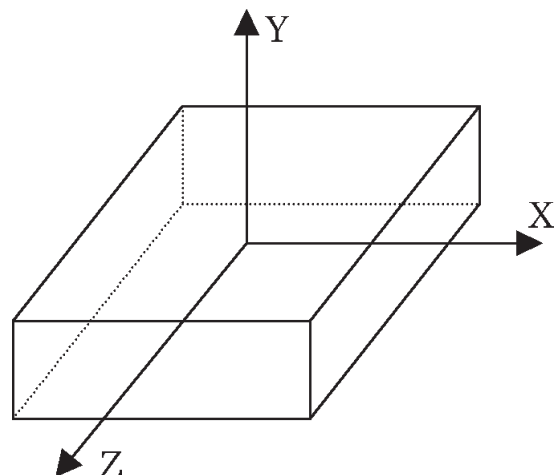
$$\begin{bmatrix} \varepsilon_x \\ \varepsilon_y \\ \gamma_{xy} \end{bmatrix} = \begin{bmatrix} \beta_{11} & \beta_{12} & 0 \\ \beta_{12} & \beta_{22} & 0 \\ 0 & 0 & \beta_{66} \end{bmatrix} \begin{bmatrix} \sigma_x \\ \sigma_y \\ \tau_{xy} \end{bmatrix} \qquad (5)$$

where the β matrix is called the reduced compliance matrix for plane strain conditions and

$$\beta_{11} = \frac{a_{11}a_{33} - a_{13}^2}{a_{33}} \qquad \beta_{12} = \frac{a_{12}a_{33} - a_{13}a_{23}}{a_{33}}$$

$$\beta_{22} = \frac{a_{22}a_{33} - a_{23}^2}{a_{33}} \qquad \beta_{66} = a_{66} \qquad (6)$$

2.2 Derivation of Strain Energy for the Elliptical Inclusion

Consider an elliptical inclusion with semi-axes 'a' and 'b' in an infinite medium, which undergoes a dilatational deformation to a similar elliptical shape with semi-axes $a(1+\delta_1)$ and $b(1+\delta_2)$ in the absence of the matrix as shown in **Figure 3(a)**. Further, assume the equilibrium boundary to be an ellipse of semi-

axes $a(1+\varepsilon_1)$ and $b(1+\varepsilon_2)$ when matrix is present, as show in **Figure 3(b)**.

Then the displacement field U_x and U_y, in the complex plane z = x + iy for the inclusion, is given by

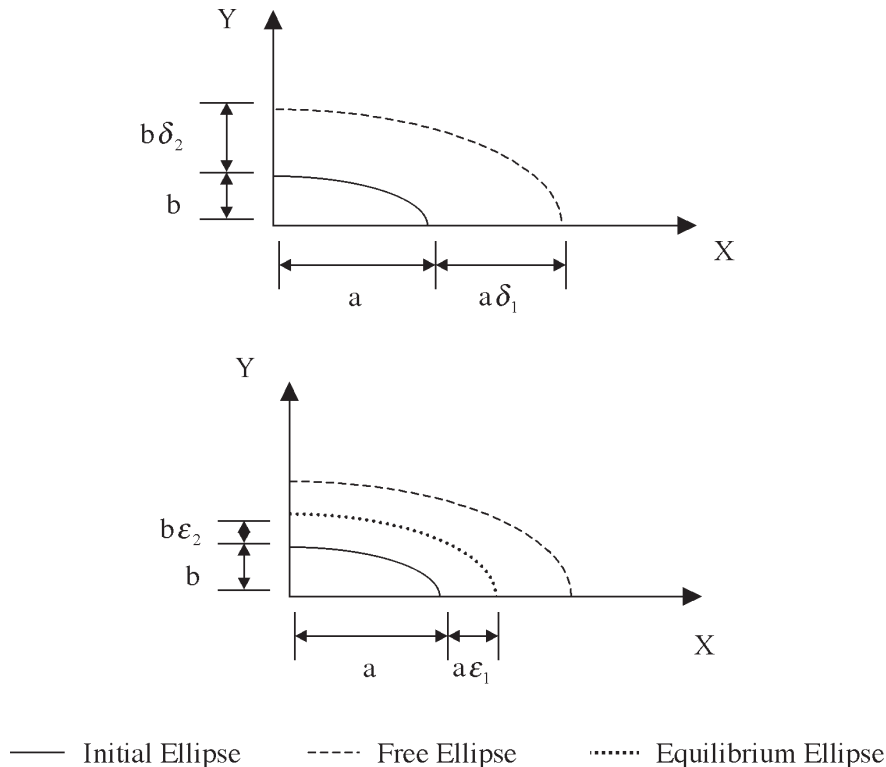$$U_x = (\varepsilon_1 - \delta_1)x \text{ and } U_y = (\varepsilon_2 - \delta_2)y \qquad (7)$$

The strains in the inclusion are

$$\varepsilon_x = (\varepsilon_1 - \delta_1) \text{ and } \varepsilon_y = (\varepsilon_2 - \delta_2) \qquad (8)$$

and the stresses in the inclusion under plane strain conditions are

$$\sigma_x = \frac{(\varepsilon_1 - \delta_1)\beta_{22} - (\varepsilon_2 - \delta_2)\beta_{12}}{\beta_{11}\beta_{22} - \beta_{12}^2}$$

$$\sigma_y = \frac{(\varepsilon_1 - \delta_1)\beta_{12} - (\varepsilon_2 - \delta_2)\beta_{11}}{\beta_{12}^2 - \beta_{11}\beta_{22}} \qquad (9)$$

$$\tau_{xy} = 0$$

Figure 3 (a) Schematic of elliptical inclusion for the case of unconstrained expansion; (b) schematic of elliptical inclusion for the case of constrained expansion

where $\beta_{11}, \beta_{22},$ and β_{12} are the components of the plane strain reduced compliance matrix defined in Equation (6), σ_x and σ_y are normal stress components and τ_{xy} is the shear stress component in the inclusion.

Substituting the stresses and strains in the strain energy density equation (Equation 10), and simplifying, we get the strain energy density in the inclusion as in Equation 11.

It should be noted that the energy density in the inclusion is uniform, i.e., independent of spatial coordinates. Hence, the total elastic strain energy (W_I) for the inclusion is obtained by multiplying the energy density of the inclusion by the area of the ellipse (assuming unit depth), giving Equation 12.

2.3 Derivation of Strain Energy for the Orthotropic Matrix

A body is called homogeneous when its elastic properties are identical in all parallel directions passing through any of its points, or in other words, all identical elements in the shape of a rectangular parallepiped with mutually parallel edges possess identical elastic properties. And a homogeneous body with three (longitudinal, radial and transverse) mutually perpendicular planes of elastic symmetry passing through every point is called an orthotropic material.

In the current study we assume the matrix (i.e. the FRP) to be a homogeneous elastic body possessing fully orthotropic properties.

According to Lekhnitskii[16] any stress function $F(x,y)$, for an orthotropic matrix, satisfies the equilibrium function, Equation 13, where, a_{11}, a_{22}, a_{12} and a_{66} are the terms of the compliance matrix and are given by Equation 14, where E_1 and E_2 are the tensile moduli along the principal directions x and y; G_{12} is the shear modulus which characterizes the change of angles between principal directions and v_{12} is the Poisson's ratio which characterizes the strain in direction y during tension in x direction.

The complex stress function $F(x, y)$ can be expressed as in Equation 15, where μ_k (k = 1, 2, 3, 4) are the roots of the characteristic equation. μ_1, μ_2, μ_3 and μ_4 could be either complex or purely imaginary but may not be real. Also, $\mu_3 = \bar{\mu}_1$ and $\mu_4 = \bar{\mu}_2$, where "bar" indicates complex conjugate.

$$\frac{1}{2}\left(\sigma_x \varepsilon_x + \sigma_y \varepsilon_y + \tau_{xy}\gamma_{xy}\right) \tag{10}$$

$$\frac{1}{2}\frac{\left(\delta_1 - \varepsilon_1\right)^2 \beta_{22} - 2\left(\delta_1 - \varepsilon_1\right)\left(\delta_2 - \varepsilon_2\right)\beta_{12} + \left(\delta_2 - \varepsilon_2\right)^2 \beta_{11}}{\beta_{11}\beta_{22} - \beta_{12}^2} \tag{11}$$

$$W_I = \frac{\pi ab}{2}\frac{\left(\delta_1 - \varepsilon_1\right)^2 \beta_{22} - 2\left(\delta_1 - \varepsilon_1\right)\left(\delta_2 - \varepsilon_2\right)\beta_{12} + \left(\delta_2 - \varepsilon_2\right)^2 \beta_{11}}{\beta_{11}\beta_{22} - \beta_{12}^2} \tag{12}$$

$$a_{22}\frac{\partial^4 F}{\partial x^4} + \left(2a_{12} + a_{66}\right)\frac{\partial^4 F}{\partial x^2 \partial y^2} + a_{11}\frac{\partial^4 F}{\partial y^4} = 0 \tag{13}$$

$$a_{22} = \frac{1}{E_2} \qquad a_{12} = \frac{-v_{12}}{E_1} \qquad \text{and} \qquad a_{66} = \frac{1}{G_{12}} \tag{14}$$

$$F(x,y) = F_1(x + \mu_1 y) + F_2(x + \mu_2 y) + F_3(x + \mu_3 y) + F_4(x + \mu_4 y) \tag{15}$$

The displacements u and v along global X and Y directions respectively, and stresses σ_x, σ_y and τ_{xy}, in an orthotropic matrix in terms of the stress function are given as[16]:

$$u(x,y) = 2\operatorname{Re}\left[p_1\phi_1(z_1) + p_2\phi_2(z_2)\right]$$
$$v(x,y) = 2\operatorname{Re}\left[q_1\phi_1(z_1) + q_2\phi_2(z_2)\right] \tag{16}$$

$$\sigma_x(x,y) = 2\operatorname{Re}\left[\mu_1^2\phi_1'(z_1) + \mu_2^2\phi_2'(z_2)\right]$$
$$\sigma_y(x,y) = 2\operatorname{Re}\left[\phi_1'(z_1) + \phi_2'(z_2)\right] \tag{17}$$
$$\tau_{xy}(x,y) = -2\operatorname{Re}\left[\mu_1\phi_1'(z_1) + \mu_2\phi_2'(z_2)\right]$$

where

$$
\begin{array}{ll}
z_1 = x + \mu_1 y & z_2 = x + \mu_2 y \\
\overline{z}_1 = x + \overline{\mu}_1 y & \overline{z}_2 = x + \overline{\mu}_2 y \\
\phi_1(z_1) = \dfrac{dF_1}{dz_1} & \phi_2(z_2) = \dfrac{dF_2}{dz_2} \\
p_1 = a_{11}\mu_1^2 + a_{12} & p_2 = a_{11}\mu_2^2 + a_{12} \\
q_1 = a_{12}\mu_1 + \dfrac{a_{22}}{\mu_1} & q_2 = a_{12}\mu_2 + \dfrac{a_{22}}{\mu_2}
\end{array}
\tag{18}
$$

2.3.1 Solution of Boundary Condition

To solve the inclusion problem, we assumed the displacement of the outer boundary of the medium to be known. Thus, the displacement Equation (16) is also the boundary condition.

The boundary of the ellipse is mapped onto a unit circle by conformal transformation[12]:

$$z = w(\zeta) \tag{19}$$

Such a mapping function is given by

$$z = \frac{a+b}{2}\frac{1}{\zeta} + \frac{a-b}{2}\zeta \tag{20}$$

Equation (20) performs the transformation of the plane with the elliptical hole into the unit circle $|\zeta| < 1$. On the boundary of this unit circle $\zeta = \sigma = e^{i\theta}$. Thus, $\sigma\overline{\sigma} = 1$, where $\overline{\sigma}$ is the complex conjugate of σ.

The displacements on the boundary of the matrix are given by

$$u = \varepsilon_1 x = \varepsilon_1\frac{z+\overline{z}}{2} \quad and \quad v = \varepsilon_2 y = \varepsilon_2\frac{z-\overline{z}}{2i} \tag{21}$$

where ε_1 and ε_2 are as defined in **Figure 3**. Transforming Equation (21) using Equation (20) on the boundary of the unit circle we get

$$u(\sigma) = \frac{\varepsilon_1 a}{2}\left(\sigma + \frac{1}{\sigma}\right) \quad and \quad v(\sigma) = \frac{i\varepsilon_2 b}{2}\left(\sigma - \frac{1}{\sigma}\right) \tag{22}$$

Equating Equation (16) and Equation (22) we get the boundary condition in terms of the displacement as

$$2\operatorname{Re}\left[p_1 A(\sigma) + p_2 B(\sigma)\right] = \frac{\varepsilon_1 a}{2}\left(\sigma + \frac{1}{\sigma}\right)$$
$$2\operatorname{Re}\left[q_1 A(\sigma) + q_2 B(\sigma)\right] = \frac{i\varepsilon_2 b}{2}\left(\sigma - \frac{1}{\sigma}\right) \tag{23}$$

where functions $A(\sigma)$ and $B(\sigma)$ are the transformed equivalent of functions $\phi_1(z_1)$ and $\phi_2(z_2)$ respectively. And, p_1, p_2, q_1 and q_2 are as defined in Equation (18).

The functions $A(\sigma)$ and $B(\sigma)$ can be determined by using the Schwartz formula below, as discussed by Savin[17]

$$X(\varsigma) = \frac{1}{2\pi i}\int_\Gamma Y(\sigma)\frac{\sigma+\varsigma}{\sigma-\varsigma}\frac{d\sigma}{\sigma} + ic_0 \tag{24}$$

where the function $X(\varsigma)$ is holomorphic inside the unit circle Γ, and $Y(\sigma)$ is the value of its real part on the contour of the unit circle. c_0 is a real constant which can be disregarded since it has no influence on the stress field.

Further, we assume

$$\mu_1 = id_1 \quad and \quad \mu_2 = id_2 \tag{25}$$

as μ_1 and μ_2 are purely imaginary roots. The two real parameters d_1 and d_2 characterize the degree of

orthotropy i.e., they characterize how much a property of a given material differs from that of an isotropic material. For the special case of isotropy, d_1 and d_2 are identical to one. Equation (18), can be thus rewritten as,

$$p_1 = a_{12} - a_{11}d_1^2 \qquad p_2 = a_{12} - a_{11}d_2^2$$

$$q_1 = \frac{a_{22} - a_{12}d_1^2}{id_1} \qquad q_2 = \frac{a_{22} - a_{12}d_1^2}{id_2} \qquad (26)$$

It can be shown that the following equation holds for the orthotropic medium,

$$a_{11}d_1^2d_2^2 = a_{22} \qquad (27)$$

Making use of Equations (25), (26) and (27) and and applying Schwartz formula (24) and Cauchy's formulae[12], we get the corresponding expressions for $A(\sigma)$ and $B(\sigma)$ from Equation (23) as follows

$$A(\sigma) = \frac{c_1\sigma}{2(d_1 - d_2)d_m}$$

$$and \quad B(\sigma) = \frac{-c_2\sigma}{2(d_1 - d_2)d_m}$$

$$(28)$$

where

$$c_1 = ad_1\varepsilon_1(a_{22} - a_{12}d_2^2) + bd_1d_2\varepsilon_2(a_{12} - a_{11}d_2^2)$$

$$c_2 = ad_2\varepsilon_1(a_{22} - a_{12}d_1^2) + bd_1d_2\varepsilon_2(a_{12} - a_{11}d_1^2)$$

$$d_m = 2a_{22}a_{12} + a_{12}^2d_1d_2 - a_{11}a_{22}(d_1^2 + d_1d_2 + d_2^2)$$

$$(29)$$

2.1.2 Strain Energy in the Matrix

The stresses in the orthotropic matrix at the interface boundary, σ_x^c, σ_y^c and τ_{xy}^c, are obtained by transforming Equation (17) and making use of Equation (28), as in Equation (30) below.

The strain energy in the matrix, W_M, due to work done at the boundary by surface traction is given by

$$W_M = \frac{1}{2}\oint(p_{nx}^c u + p_{ny}^c v)ds \qquad (31)$$

where ds is the element of arc length. The surface tractions p_{nx}^c and p_{ny}^c are given by

$$p_{nx}^c = \sigma_x^c \cos(x,n) + \tau_{xy}^c \cos(y,n)$$
$$p_{ny}^c = \tau_{xy}^c \cos(x,n) + \sigma_y^c \cos(y,n)$$
$$(32)$$

where n is the outward drawn normal.

Solving the integral Equation (31) using Equations (30) and (32) we get an expression for total strain energy in the matrix

$$W_M = \frac{-\pi}{2d_m}\Big[\varepsilon_1^2 a^2 a_{22}(d_1 + d_2)$$

$$+2ab\varepsilon_1\varepsilon_2(a_{22} + a_{12}d_1d_2) + \varepsilon_2^2 b^2 a_{11}d_1d_2(d_1 + d_2)\Big]$$

$$(33)$$

2.2 Equilibrium Configuration

The total energy of the elastic inclusion-matrix system is obtained by scalar addition of W_I and W_M, from Equations (12) and (33) and is given by Equation (34).

$$\sigma_x^c = \frac{-1}{(d_1 - d_2)d_m}\left[\frac{c_1d_1^2\{(a - d_1b) - (a + d_1b)\cos 2\theta\}}{(a^2 + d_1^2b^2) - (a^2 - d_1^2b^2)\cos 2\theta} - \frac{c_2d_2^2\{(a - d_2b) - (a + d_2b)\cos 2\theta\}}{(a^2 + d_2^2b^2) - (a^2 - d_2^2b^2)\cos 2\theta}\right]$$

$$\sigma_y^c = \frac{1}{(d_1 - d_2)d_m}\left[\frac{c_1\{(a - d_1b) - (a + d_1b)\cos 2\theta\}}{(a^2 + d_1^2b^2) - (a^2 - d_1^2b^2)\cos 2\theta} - \frac{c_2\{(a - d_2b) - (a + d_2b)\cos 2\theta\}}{(a^2 + d_2^2b^2) - (a^2 - d_2^2b^2)\cos 2\theta}\right] \qquad (30)$$

$$\tau_{xy}^c = \frac{-1}{(d_1 - d_2)d_m}\left[\frac{c_1d_1(a + d_1b)\sin 2\theta}{(a^2 + d_1^2b^2) - (a^2 - d_1^2b^2)\cos 2\theta} - \frac{c_2d_2(a + d_2b)\sin 2\theta}{(a^2 + d_2^2b^2) - (a^2 - d_2^2b^2)\cos 2\theta}\right]$$

Samit Roy, G.H. Nie, R. Karedla and L. Dharani

$$W = \frac{\pi ab}{2} \frac{(\delta_1 - \varepsilon_1)^2 \beta_{22} - 2(\delta_1 - \varepsilon_1)(\delta_2 - \varepsilon_2)\beta_{12} + (\delta_2 - \varepsilon_2)^2 \beta_{11}}{\beta_{11}\beta_{22} - \beta_{12}^2}$$

$$+ \frac{-\pi}{2d_m} \left[\varepsilon_1^2 a^2 a_{22}(d_1 + d_2) + 2ab\varepsilon_1\varepsilon_2(a_{22} + a_{12}d_1d_2) + \varepsilon_2^2 b^2 a_{11}d_1d_2(d_1 + d_2) \right] \tag{34}$$

$$\varepsilon_1 = \frac{\varepsilon_1^N}{\varepsilon^D} \qquad \varepsilon_2 = \frac{\varepsilon_2^N}{\varepsilon^D} \tag{35}$$

$$\varepsilon_1^N = \left(\frac{b}{a}\right) \left\{ \left[\beta_{12}(a_{22} + d_1d_2a_{12}) - d_m + \left(\frac{b}{a}\right)\beta_{22}a_{11}d_1d_2(d_1 + d_2) \right] \delta_1 \right.$$

$$- \left[\beta_{11}(a_{22} + d_1d_2a_{12}) + \left(\frac{b}{a}\right)\beta_{12}a_{11}d_1d_2(d_1 + d_2) \right] \delta_2 \right\}$$

$$\varepsilon_2^N = -\left[\left(\frac{b}{a}\right)\beta_{22}(a_{22} + d_1d_2a_{12}) + \beta_{12}a_{22}(d_1 + d_2) \right] \delta_1$$

$$+ \left\{ \beta_{11}a_{22}(d_1 + d_2) + \left(\frac{b}{a}\right) \left[\beta_{12}(a_{22} + d_1d_2a_{12}) - d_m \right] \right\} \delta_2 \tag{36}$$

$$\varepsilon^D = \left(\frac{b}{a}\right) \left[d_1d_2(\beta_{11}\beta_{22} - \beta_{12}^2) - d_m \right] + 2\left(\frac{b}{a}\right)(a_{22} + d_1d_2a_{12})\beta_{12}$$

$$+ \beta_{11}a_{22}(d_1 + d_2) + \left(\frac{b}{a}\right)^2 \beta_{22}a_{11}d_1d_2(d_1 + d_2)$$

Minimizing W with respect to ε_1 and ε_2, and solving for them we get Equation (35) (see also Equation (36)).

The stresses in the inclusion are derived by substituting Equations (35) and (36) in Equation (9). The inclusion stress σ_x and σ_y are both compressive stresses and are spatially uniform. However, the compressive stress σ_y gives rise to a stress concentration at the tip of the ellipse and could potentially act as a crack driving force (see **Figure 1**) as will be discussed in the next section.

3. MODELING OF DELAMINATION CAUSED BY FREEZE-THAW

3.1 Stress Intensity Factor for Slender Ellipses

For the region of the notch tip where 'r' is small compared with other planar dimensions, the stress field becomes[18] Equation (37).

where ρ (radius of curvature of the notch), r and θ are as defined in **Figure 4**, and K_I is the Mode I stress intensity factor.

$$\sigma_x = -\frac{K_I}{\sqrt{2\pi r}} \frac{\rho}{2r} \cos\frac{3\theta}{2} + \frac{K_I}{\sqrt{2\pi r}} \cos\frac{\theta}{2} \left[1 - \sin\frac{\theta}{2}\sin\frac{3\theta}{2} \right]$$

$$\sigma_y = +\frac{K_I}{\sqrt{2\pi r}} \frac{\rho}{2r} \cos\frac{3\theta}{2} + \frac{K_I}{\sqrt{2\pi r}} \cos\frac{\theta}{2} \left[1 + \sin\frac{\theta}{2}\sin\frac{3\theta}{2} \right] \tag{37}$$

$$\tau_{xy} = -\frac{K_I}{\sqrt{2\pi r}} \frac{\rho}{2r} \sin\frac{3\theta}{2} + \frac{K_I}{\sqrt{2\pi r}} \sin\frac{\theta}{2}\cos\frac{\theta}{2}\cos\frac{3\theta}{2}$$

Figure 4 Slender notch

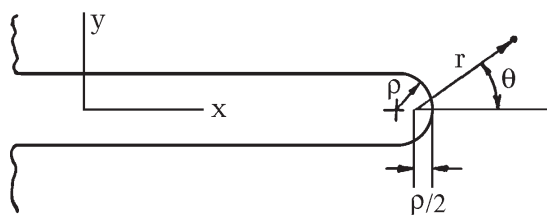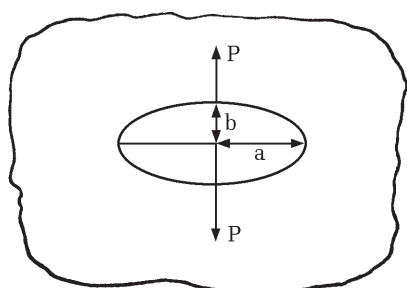**Figure 5 Elliptical hole with remotely applied stress**

Figure 6 Ellipse in an infinite sheet with symmetrical splitting forces P
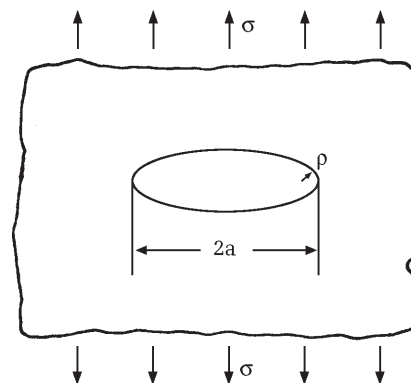
Figure 7 Crack face loaded by distributed traction force

For the elliptical hole shown in **Figure 5**, as $\rho \rightarrow 0$ we recover the sharp crack tip. Extending the above result, Equation (37), to an elliptical hole through a wide plate where the semi-major axis, a, is perpendicular to a remotely applied tension stress, σ, the comparable crack solution obtained as $\rho \rightarrow 0$ is given by,

$$K_I = \sigma \sqrt{\pi a} \tag{38}$$

For a crack in a large plate of thickness B loaded by equal and opposite point forces, P, on the surface of the crack at a distance d from the centre of the crack, the stress intensity factor is

$$K_I = \frac{2}{\sqrt{\pi}} \frac{P}{B} \frac{\sqrt{a}}{\sqrt{a^2 - d^2}} \tag{39}$$

Solutions for distributed loads on the crack face may be obtained by expressing P, in **Figure 6**, as due to a local pressure P_ξ acting at a distance ratio $\xi = 1\text{-}c/a$ from the center, where c is as defined in **Figure 7**.

The incremental stress intensity dK_I at the crack tip due to this force is[19]:

$$dK_I = \frac{2 p_\xi}{\pi} \frac{d\xi}{\sqrt{1 - \xi^2}} \sqrt{\pi a} \tag{40}$$

and for an arbitrary distribution from ξ_1 to ξ_2:

$$K_I = \sqrt{\pi a}\, \frac{2}{\pi} \int_{\xi_1}^{\xi_2} \frac{p_\xi d\xi}{\sqrt{1 - \xi^2}} \tag{41}$$

For the special case when $p_\xi = \sigma_y$, i.e, a uniform pressure loading on the crack face,

$$K_I = \sigma_y \sqrt{\pi a} \tag{42}$$

which shows that the stress intensity factor for a uniform pressure over the crack face is exactly equivalent to that due to a uniform stress remote from the crack.

Unfortunately, the exact solution for the Mode I stress intensity for the case of ice inclusion within a crack, as depicted by **Figure 7**, cannot be obtained using Equation (41) because the analytical form of the actual stress distribution, P_ξ, on the crack boundaries is mathematically intractable. However, it is hereby postulated that an approximate solution for the Mode I stress intensity factor for the crack

Figure 8 Slender ellipse-crack equivalence diagram
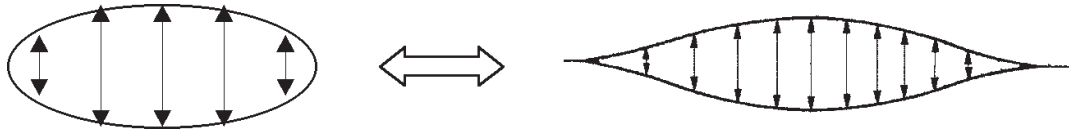
may be obtained by assuming that the actual stress distribution, P_ξ, may be replaced by an uniform stress distribution, σ, due to an elliptical ice inclusion having the same length and width as the original crack, as shown schematically in **Figure 8**. Thus, after the uniform normal stress σ, has been obtained for the equivalent elliptical inclusion using Equation (9), this uniform traction can then be used in Equation (42) to obtain the approximate Mode I stress intensity factor for the crack with ice inclusion.

2.2 Life Prediction for Freeze-Thaw Cycles

Freeze-thaw cycles could be an important reason for crack growth in an inclusion-matrix system. If the plastic zone at the crack tip is sufficiently small, for a growing crack in the presence of a constant-amplitude cyclic stress intensity, the conditions at the crack tip are uniquely defined by the current K_I value. Functionally the crack growth law can be expressed as[20]

$$\frac{da}{dN} = f(\Delta K) \tag{43}$$

where $\Delta K = K_{max} - K_{min}$ and da/dN is the crack growth per cycle.

The relation between da/dN and ΔK was given by the Paris Law,

$$\frac{da}{dN} = C(\Delta K)^m \tag{44}$$

where C and m are material constants that are determined experimentally. Also, Equation (44) is valid only in the linear region of the $\log(da/dN)$ Vs $\log(\Delta K)$ graph.

The number of stress cycles (N_f) required to propagate a crack from an initial length, a_0, to a final length, a_f, is given by:

$$N_f = \int_{a_0}^{a_f} \frac{da}{C(\Delta K)^m} \tag{45}$$

For the present problem, the total number of cycles, N_f, for a crack to grow from a_0 to a_f is estimated by substituting K_I (Equation (42)) for ΔK in Equation (45):

$$N_f = \int_0^{N_f} dN = \int_{a_i}^{a_f} \frac{da}{C(K_I)^m} \tag{46}$$

4. CONCLUSIONS

An analytical formulation to calculate the stress intensity factor K_I due to ice inclusion within a crack in both transversely isotropic and orthotropic matrices was presented. The formulation combines elasticity solutions for elliptical inclusions with established concepts of fracture mechanics. It was postulated that an approximate solution for the Mode I stress intensity factor for the crack may be obtained by assuming that the actual normal stress distribution on the crack face, P_ξ, may be replaced by an uniform stress distribution, σ, due to an elliptical ice inclusion having the same length and width as the original crack. A life prediction methodology for cyclic crack growth due to freeze-thaw was also developed. The verification of the analytical model predictions and some potential applications will be presented in a separate paper.

REFERENCES

1.   Verghese, K. N. E., Morrell, M. R., Horne, M. R. and Lesko, J., J., Freeze-thaw durability of polymer matrix composites in infrastructure. Proceedings of the Fourth International Conference on Durability Analysis of Composite Systems, Duracosys 99, Brussels, Belgium, (1999).

2.   Lord, H., W. and Dutta, P. K., On the design of polymeric composite structures for cold regions

applications. Journal of Reinforced Plastics and Composites, 7, (1988), 435-458.

3. Dutta, P. K., Structural fibre composite material for cold regions. Journal of Cold Regions Engineering, 2, No. 3, (1988),124-134.

4. Goodier, J. N., Concentration of stress around spherical and cylindrical inclusions and flaws. Transactions ASME, 55, (1933), 39-44.

5. Donnell, L. H., Theodore von Kármán Anniversary Volume, Pasadena, (1941).

6. Eshelby, J. D., The determination of the elastic field of an ellipsoidal inclusion, and related problems. Proc. Roy. Soc. A241, (1957), 376.

7. Eshelby, J. D., Elastic inclusion and inhomogeneities. In Progress in Solid Mechanics 2, ed. I. N. Sneddon and R. Hill, North Holland, Amsterdam, (1961), 89-140.

8. Jaswon, M. A. and Bhargava, R. D., Two dimensional elastic inclusion problems. Proceedings of the Cambridge Philosophical Society, 57, (1961), 669-680.

9. Bhargava, R. D. and Radhakrishna, H. C., Two-dimensional elliptic inclusions. Proc. Camb. Phil. Soc., 59, (1963), 811.

10. Aderogba, K. V. and Berry, D. S., Inclusions in a two-phase elastic space-plane circular and rectangular inclusions. Journal of Mechanics and Physics of Solids, 19, (1971), 285-293.

11. Toya, M., A crack along the interface of a rigid circular inclusion embedded in an elastic solid. International Journal of Fracture, 9, No. 4, (1973), 463-470.

12. Mushkelishvili, N. I., Some basic problems of the mathematical theory of elasticity. Groningen Publisher, (1953).

13. Toya, M., A crack along the interface of a circular inclusion embedded in an infinite solid. Journal of Mechanics and Physics of Solids, 22, (1974), 325-348.

14. Love, A. E. H., The Mathematical Theory of Elasticity, 4th Edn. Cambridge Publisher, (1927).

15. Jones, R. M., Mechanics of Composite Material, 2nd Edn. Taylor and Francis, New York, (1999).

16. Lekhnitskii, S., G., Anisotropic plates. Gordon and Breach Science Publishers, New York, (1968).

17. Savin, G. N., Stress Concentration Around Holes. Pergamon Press, New York, (1961).

18. Tada, H., Paris, P. C. and Irwin, G., R., Stress analysis of cracks handbook. Del Research Corporation, New York (1973).

19. Williams, J. G., Fracture mechanics of polymers. Ellis Horwood Limited, Chichester, (1984).

20. Anderson, T. L., Fundamentals and Applications of Fracture Mechanics, 2nd Edn. CRC Press, Inc., Boca Raton (1995).

ACKNOWLEDGEMENT

Stress Intensity Factor for an Elliptic Inclusion in Orthotropic Laminates Subjected to Freeze-thaw: Model Verification

Samit Roy*, G.H. Nie*, R. Karedla**, L. Dharani**

*Mechanical and Aerospace Engineering Department, Oklahoma State University
**Mechanical and Aerospace Engineering Department, University of Missouri-Rolla

SUMMARY

Verifications and applications of an analytical model developed previously for the calculation of mode-I stress intensity factor of a pre-existing crack in an orthotropic composite structure due to the phase transition of trapped moisture are presented in this paper. The verifications are based on comparisons of the stresses in an elliptic elastic inclusion and the stress intensity factor with a special case of isotropy (for which there exists an analytical solution) and with finite element analysis for the case of orthotropy. The results indicate that the stress state in a slender elliptic elastic inclusion can be used to approximate the stress field at the crack face, which could subsequently be adopted to determine the stress intensity factor. Analyses of the delamination and fatigue life prediction for freeze-thaw cycling are provided as specific applications of the model.

1. INTRODUCTION

Motivation for the present study originates from the fact that composite materials are being progressively used in cold temperature environments. The existence of interfacial cracks and freezability of moisture in these cracks has been established by several researchers, and a detailed overview has been presented in a companion paper[1]. A review of the literature shows that although considerable work has been done on stress fields in structures with inclusions, a framework for the fracture mechanics analysis of freeze-thaw cycling in orthotropic composite structures is yet to be established. In addition, a guideline for conditions of crack growth in composites due to freezing is necessary for safe structural design.

Multiple defects exist (e.g. cracks, inhomogeneities, etc.) in most composites laminates. It is desirable that mechanical behavior of materials and structures are determined exactly by using effective approaches. But, because of mathematical intractability, many such problems cannot be solved analytically except in few special cases, e.g., defects occurring in a regular array, or simple shapes, etc. However, numerical calculations have shown that for two inhomogeneities embedded in two-dimensional and three-dimensional isotropic or anisotropic elastic media[2-5], the interaction between the inhomogeneities becomes negligible when the distance between them is larger than about four times the characteristic length of inhomogeneity. In other words, results from the analysis of a single inhomogeneity remain valid for numerous defects if the distance between any two defects is larger than four times the characteristic length of the defect.

It is well known that a slender ellipse can, in the limit, simulate a crack. Our research therefore focuses on an elliptic inclusion (inhomogeneity) embedded in orthotropic laminates. Wang et. al[6] have investigated delamination induced by a single crack, i.e. an intra-ply transverse crack or an inter-ply transverse crack in composite laminates. To our knowledge, an analytical solution to an inclusion in an orthotropic matrix has not been developed. Actually, investigations on voluminal inhomogeneity other than crack (without any volume), are relatively few because of difficulty in developing closed form solutions. Especially, the extension of the corresponding solution to problems in the area of anisotropic and composite materials is, undoubtedly, a formidable and challenging task. We have attempted to obtain a simple yet elegant form of the solution for the stress state in the inclusion, as described in a companion paper[1]. The main focus of this manuscript is on verification and application of the proposed model. The verification is based on comparisons

with a special case of isotropy (for which there exists an analytical solution) and with finite element analysis for the orthotropic case.

It should be noted that the solution for single defect (crack) is of great importance in the analysis of both isotropic and anisotropic materials. This is because initially several initiation sites (imperfections) may evolve, and then small defects (cracks) will coalesce to produce large defects (cracks), and eventually one dominant defect (crack) will reach a maximum allowable size. Furthermore, commonly used methods for multiple defects are based on elastic fields of the single defect [7,8].

The objective of this paper is to provide benchmark verifications of a proposed analytical model[1] for the calculation of the stress intensity factor (KI) of a pre-existing crack in a composite structure due to the phase transition of trapped moisture. The constrained volume expansion of trapped moisture due to freezing is postulated to be the crack driving force. The principle of minimum strain energy is employed to calculate the elastic field within an orthotropic laminate containing an idealized elliptical elastic inclusion in the form of ice. It is postulated that a slender elliptic elastic inclusion could be used to approximate the stress field at the crack face, which could subsequently be used to calculate the stress intensity factor, KI, for the crack. Benchmark verifications of the analytical model predictions and some specific applications regarding static and fatigue failure caused by freeze-thaw are presented in this paper.

2. RESULTS AND APPLICATION

The analytical derivation presented in a companion paper[1] is benchmarked using finite element analysis (FEA). The J-integral contour is calculated using FEA. Since the J-integral is equal to the strain energy release rate, G, for an elastic material, the stress intensity K_I is calculated using the following approach. The energy release rate, G, quantifies the net change in potential energy that accompanies an increment of crack extension. The stress intensity factor, K, characterizes the stresses, the strains and the displacements near the crack tip. The energy release rate describes global behavior, while K is a local parameter. For linear elastic isotropic materials, K and G are uniquely related through the elastic modulus E and Poisson's ratio ν as,

$$G_I = \frac{K_I^2}{E'} \qquad (1)$$

where E′ = E for plane stress

and $E' = \dfrac{E}{1 - \nu^2}$ for plane strain

Linear Elastic Fracture Mechanics (LEFM) can be applied to anisotropic bodies with cracks in the same way as it is for isotropic material. The relation between G and K for an orthotropic body in plane stress Mode–I loading is given by [9],

$$G_I = K_I^2 \left(\frac{a_{11} a_{22}}{2} \right)^{\frac{1}{2}} \left[\left(\frac{a_{22}}{a_{11}} \right)^{\frac{1}{2}} + \frac{2a_{12} + a_{66}}{2a_{11}} \right]^{\frac{1}{2}} \qquad (2)$$

where, the a_{ij}'s are the components of the compliance matrix for orthotropic elastic body. A solution for plane strain formulation is obtained by replacing a_{ij} in Equation (2) by β_{ij} (also see equation (6) in Roy et al[1]), where ,

$$\beta_{ij} = a_{ij} - \frac{a_{i3} a_{j3}}{a_{33}} \quad i, j = 1, \dots, 6 \qquad (3)$$

The strain energy release rate calculated using finite element analysis (FEA) are converted to appropriate stress intensity factor using Equations (1) and (2), and then compared with the K_I from the analytical derivation.

3. FINITE ELEMENT MODELING

The modeling is performed using a commercial finite element package, ABAQUS, and the finite element mesh is developed using I-DEAS pre-processor graphics software. Two separate inclusion configurations are modeled: (a) elliptic inclusion with blunt tip (shown in **Figure 1**) and (b) inclusion with sharp crack tip (shown in **Figure 2**). Here, "a" defines the length of the semi-major axis of the ellipse shown in **Figure 1**, and also the length of the crack shown in **Figure 2**; "b" defines the length of the semi-minor axis of the ellipse in **Figure 1**, and also the height of the inclusion in **Figure 2**. For each of these configurations, five cases each with different a/b ratios (a/b = 3, 6, 10, 15, 30 or b/a = 0.33, 0.16, 0.1, 0.06, 0.03) are modeled. The dimension of the surrounding matrix medium, 0.25 m x 0.5 m, is kept constant to simulate the infinite elastic plane assumed in the analytical derivation[1]. The semi-major axis, a, of the ellipse and the crack is also held constant at 0.03m. Only the semi-minor axis, b is changed accordingly to obtain the desired a/b ratio.
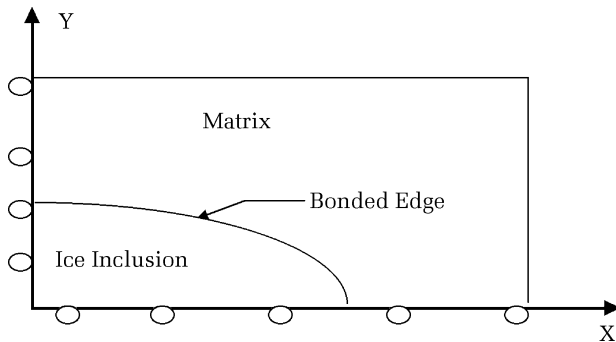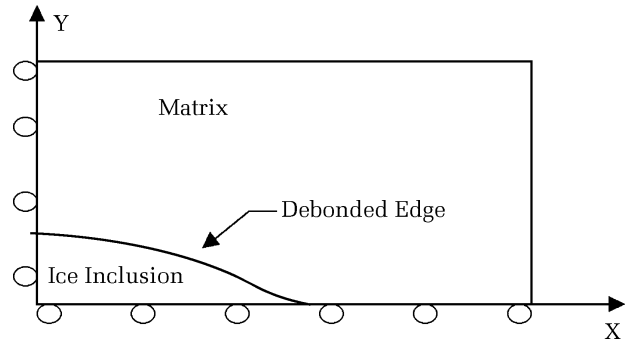
Figure 1. FEA model of blunt elliptical inclusion

**Figure 2. FEA model of inclusion with sharp crack tip**

Eight node isoparametric plane-strain quadrilateral elements are used in all the FEA cases. For the elliptical inclusion case, the ice and the orthotropic matrix are modeled with bonded common edge, as shown in **Figure 1**. However, in the sharp crack inclusion model, the interface between the matrix and the inclusion is modeled as a fully debonded surface to facilitate numerical convergence of the J-integrals computed along different contours (see **Figure 3**). The crack surface is modeled using slave and master contact surface option available in ABAQUS. Invoking symmetry about both global X and Y axis, only one quarter of the inclusion is modeled. Roller supports are applied on all nodes along the X and Y axis as boundary conditions for the problem depicted in **Figures 1 and 2**.

In ABAQUS, several concentric contours integral evaluations need to be performed at the crack tip for the accurate computation of J-integral. Each contour is a ring of elements completely surrounding the crack tip from one crack face to the opposite crack face, as shown in **Figure 3**. ABAQUS automatically finds the elements that form each ring from the node given as the crack tip from one crack face to the other. Hence, it is necessary to specify the number of contours to be used in calculating the J-integral.

The analysis requires the node number of the crack tip. It is also necessary to provide the direction cosine of the crack front, which is input into ABAQUS as the crack extension direction. In the case of the sharp crack, the inverse square root singularity at the crack

Figure 3. Focused mesh in ABAQUS for J-integral evaluation
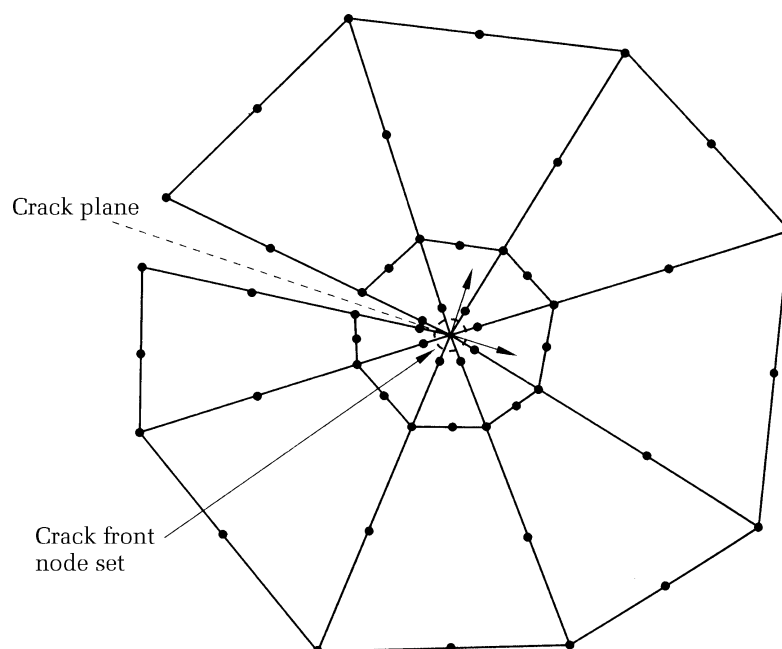
tip is introduces in order to improve the accuracy of the J-integral. This is achieved by collapsing the quadrilateral elements nearest to the crack tip into a focused mesh of triangular elements, and by moving the element mid-side nodes to the quarter-point as illustrated in **Figure 3**. The computed value of the J-integral from each of the contours is in close agreement, thereby indicating convergence of the J-integral.

The Carbon/Epoxy composite used in the benchmark analyses is T300/5208 with the following in-plane orthotropic material properties,

$$E_1 = 181 \text{ GPa} \qquad G_{12} = 7.17 \text{ GPa}$$
$$E_2 = 10.3 \text{ GPa} \qquad \nu_{12} = 0.28 \qquad (4)$$

In the FEA model, the ice formation process is simulated by an equivalent material expansion due to a unit change in temperature. Since freezing occurs at constant temperature (0° C for water) there is no expansion or contraction in the surrounding matrix during this process. Therefore, the linear expansion for the matrix is taken as zero during freezing. The only change in geometry is due to the expansion within the solid inclusion due to a phase transition from water to ice. The isotropic material properties of the ice inclusion used for the analysis are

$$E = 10.3 \text{ GPa}$$
$$\nu = 0.33$$
$$\alpha = 0.029 \text{ m/°C} \qquad (5)$$

where α is the effective coefficient of linear expansion of water when it freezes to form ice.

4. BENCHMARK RESULTS FOR TRANSVERSELY ISOTROPIC PROBLEM

For the purposes of verifying analytical results presented in the companion paper[1], first, the orthotropic matrix formulation is benchmarked by simplifying the formulation to isotropic matrix material (refer to Equation (35), Roy et al[1]), and results are compared with known analytical solutions by Bhargava et al[1°]. Then, the present results are also benchmarked using FEA solutions for a specific transversely isotropic matrix.

The expressions for stresses, and displacements in an elliptical inclusion embedded in an isotropic matrix, as derived by Bhargava et al[1°] are written as follows,

$$\sigma_x = \lambda_1 (\varepsilon_1 + \varepsilon_2 - \delta_1 - \delta_2) + 2\mu_1 (\varepsilon_1 - \delta_1)$$
$$\sigma_y = \lambda_1 (\varepsilon_1 + \varepsilon_2 - \delta_1 - \delta_2) + 2\mu_1 (\varepsilon_2 - \delta_2)$$
$$\tau_{xy} = 0$$
$$U_x = (\varepsilon_1 - \delta_1)x$$
$$U_y = (\varepsilon_2 - \delta_2)y \qquad (6)$$

where

$$\varepsilon_1 = \frac{\varepsilon_1^N}{\varepsilon^D}; \quad \varepsilon_2 = \frac{\varepsilon_2^N}{\varepsilon^D} \qquad (7)$$

$$\varepsilon_1^N = b\Big[\delta_1\big\{b\mu(\kappa+1)(\lambda_1+2\mu_1) + 4\mu_1\kappa(\lambda_1+\mu_1)a - \lambda_1\mu(\kappa-1)a\big\}$$
$$+ \mu\delta_2\big\{\lambda_1(\kappa+1)b - (\lambda_1+2\mu_1)(\kappa-1)a\big\}\Big]$$

$$\varepsilon_2^N = a\Big[\delta_2\big\{a\mu(\kappa+1)(\lambda_1+2\mu_1) + 4\mu_1\kappa(\lambda_1+\mu_1)b - \lambda_1\mu(\kappa-1)b\big\}$$
$$+ \mu\delta_1\big\{\lambda_1(\kappa+1)a - (\lambda_1+2\mu_1)(\kappa-1)b\big\}\Big]$$

$$\varepsilon^D = 4ab\Big[\mu^2 + \mu_1\kappa(\lambda_1+\mu_1)\Big] + \lambda_1\mu\Big[\kappa(a-b)^2 + (a+b)^2\Big]$$
$$+ 2\mu_1\mu(\kappa+1)(a^2+b^2) \qquad (8)$$

where λ_1, μ_1 and λ, μ are the two pairs of Lame constants of the inclusion and matrix materials, respectively, and $\kappa = 3 - 4\nu$, ν being Poisson's ratio for the matrix. The two parameters δ_1 and δ_2 as defined in Roy et al[1], correspond the dilatational deformations in x- and y- directions, respectively. The stresses and displacements in the inclusion obtained from orthotropic formulation are compared with isotropic formulations (i.e., Equations (6) and (7)) and FEA. The properties of ice given by Equation (5) are used, and the following materials constants for a specific transversely isotropic composite material, T300/5208, are applied in the calculations for stress fields, as stated in Equation (9) and Equation (35) presented in Roy et al[1]:

$$E_1 = 10.3 \text{ GPa} \quad \nu_{12} = 0.56 \quad G_{12} = 3.3 \text{ GPa}$$
$$E_2 = 10.3 \text{ GPa} \quad \nu_{13} = 0.16 \quad G_{12} = 7.17 \text{ GPa} \quad (9)$$
$$E_3 = 181 \text{ GPa} \quad \nu_{23} = 0.16 \quad G_{12} = 7.17 \text{ GPa}$$

Table 1 shows a comparison between the formulation reduced from the present analytical orthotropic formulation by assuming isotropic matrix material, and the known isotropic formulation[1°] for the case of elliptic inclusion with blunt tip, as shown in **Figure 1**. **Table 2** presents a comparison between orthotropic formulation, for the transversely isotropic matrix material, as mentioned above, and FEA results for the elliptic inclusion case with blunt tip. **Figures 4 and 5** are the plots of the transverse stress s_y and axial stress s_x in the elliptic ice inclusion. It can be observed that

Table 1. Comparison of stresses for isotropic formulation and a blunt elliptic inclusion

b/a	Stress σ_x (MPa)		Stress σ_y (MPa)	
	Present	Bhargava et al[3]	Present	Bhargava et al[10]
0.033	-324.49530	-324.49540	-10.70837	-10.70839
0.066	-314.45000	-314.45000	-20.75369	-20.75365
0.10	-304.73060	-304.73060	-30.47311	-30.47306
0.166	-287.48170	-287.48170	-47.72193	-47.72195
0.333	-251.46560	-251.46560	-83.73804	-83.73805

Table 2. Comparison of stresses with FEA for a blunt elliptic inclusion in orthotropic matrix

b/a	Stress σ_x (MPa)		Percentage Error	Stress σ_y (MPa)		Percentage Error
	Present	FEA		Present	FEA	
0.033	-320.75	-323.45	0.83	-9.44	-9.48	0.42
0.066	-307.62	-309.85	0.72	-18.24	-18.31	0.38
0.10	-295.27	-297.44	0.73	-26.72	-26.56	0.60
0.166	-274.17	-275.64	0.53	-41.70	-41.56	0.34
0.333	-233.02	-233.75	0.31	-72.99	-72.43	0.77

Figure 4. Comparison of transverse stress σ_y for transversely isotropic matrix
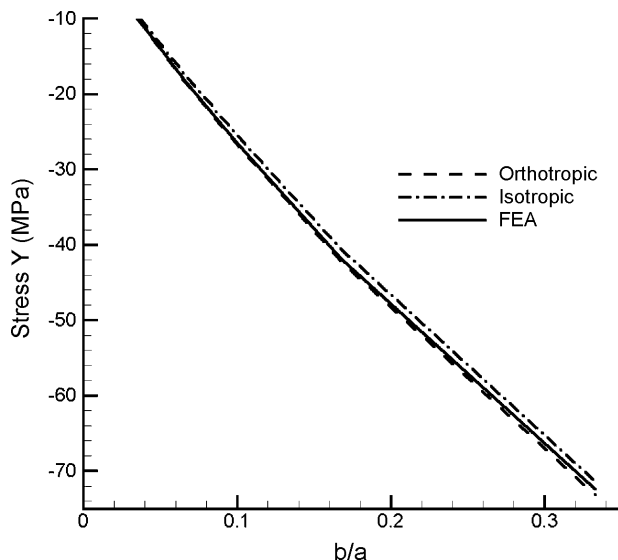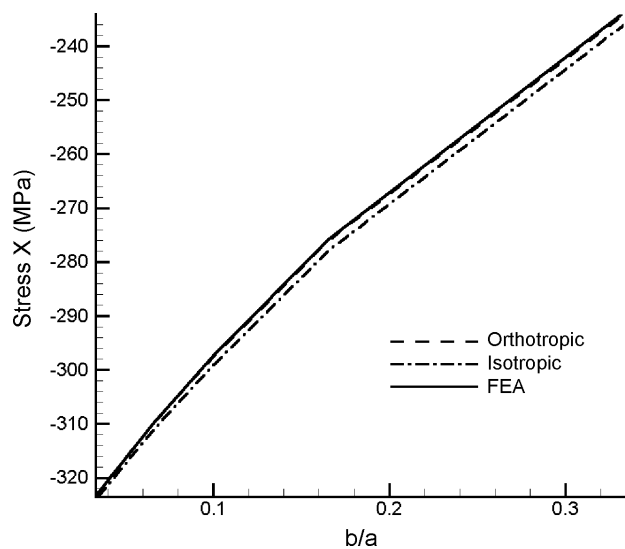

Figure 5. Comparison of axial stress σ_x for transversely isotropic matrix

the present results are almost exactly the same as that from Bhargava et al[10] for the case that the matrix material is isotropic. Excellent agreement with numerical FEA results is also observed.

In addition to inclusion stresses, a comparison of predicted displacements in the inclusion is also performed. **Figures 6 and 7** are the plots of displacements in the X- and Y- directions

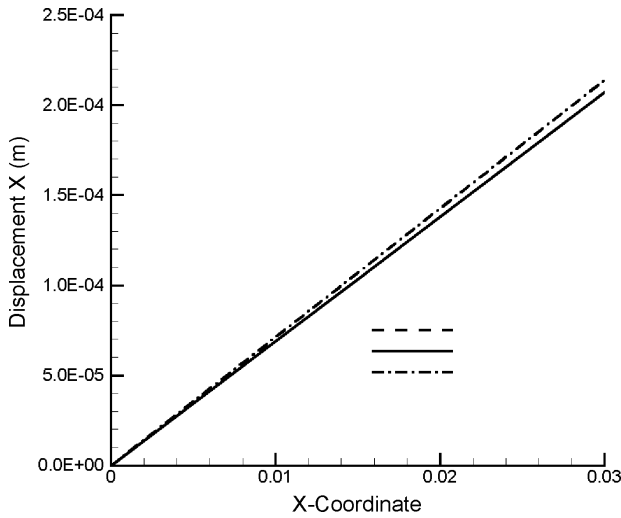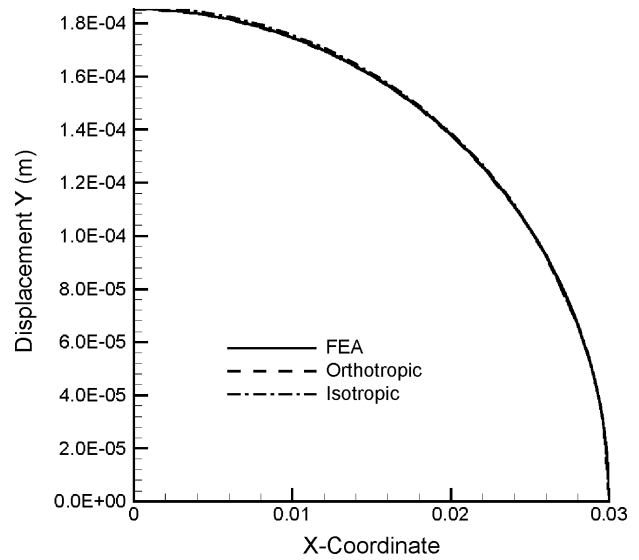**Figure 6. Comparison of X-displacement for transversely isotropic matrix, b/a =0.16**

**Figure 7. Comparison of Y-displacement for transversely isotropic matrix b/a = 0.16**

respectively, i.e. U_x, U_y, along the boundaries of the elliptic inclusion for the case b/a = 0.16. It can be seen that the predicted displacements are in good agreement with FEA results.

5. ELLIPSE-CRACK EQUIVALENCE FOR A TRANSVERSELY ISOTROPIC MATRIX

Clearly, the exact solution for the Mode I stress intensity for the case of ice inclusion within an open crack, as depicted by **Figure 2**, cannot be obtained directly because of the fact that the determination of the actual stress distributions on the crack boundaries is mathematically intractable. However, it is hereby postulated that an approximate solution for the Mode I stress intensity factor for the crack may be obtained by assuming that the actual stress distribution on the crack face, p_ξ, may be reasonably replaced by an uniform stress distribution, σ_y, due to an elliptic ice inclusion having the same length and width as that of the original crack, as discussed in Roy et al[1]. Thus, the resulting uniform normal stress, σ_y, can be applied to determine the Mode I stress intensity factor for the crack.

To verify the validity of such an analogy, some comparisons are presented. The transverse stress in the inclusion, σ_y, obtained from the analytical solution for the elliptic notch **(Figure 1)**, and the transverse stress for the inclusion with a sharp tip **(Figure 2)** obtained from FEA are plotted on the same scale along the semi-major axis, as shown in

Figure 8. Comparison of transverse stress plot for b/a = 0.03
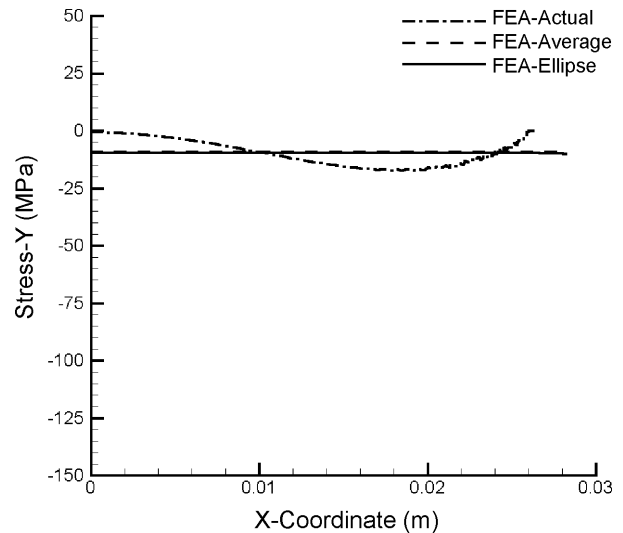
Figures 8-12. It is observed that for the crack case, the stress is roughly in the shape of a cosine curve (referred to as FEA-Actual) with its mean value (referred to as FEA-Average) close to the transverse stress (referred to as FEA-Ellipse) predicted for an equivalent elliptic inclusion having the same a/b ratio. Based on these observations, the transverse stress, σ_y, derived for an elliptic inclusion is employed to evaluate the stress intensity factor for a crack with the same a/b ratio.

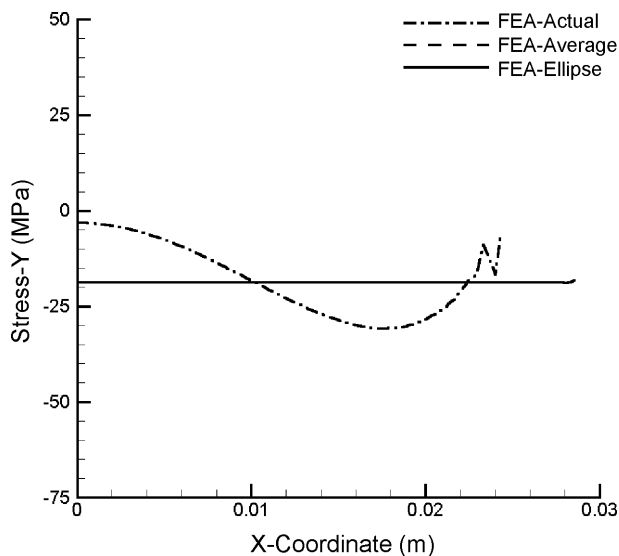**Figure 9. Comparison of transverse stress plot for b/a = 0.06**

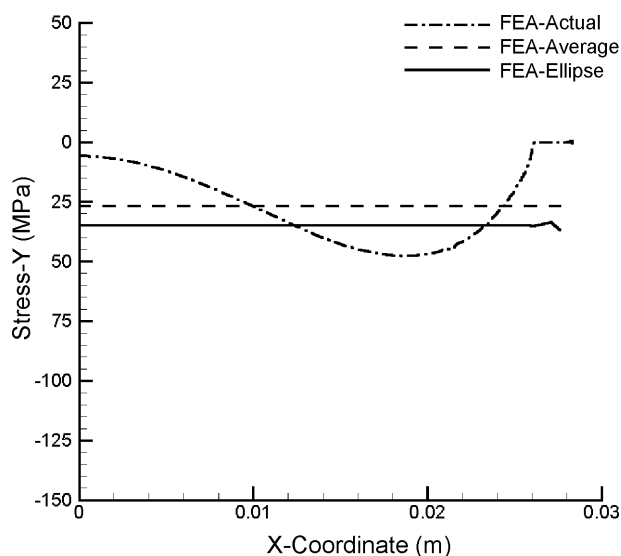**Figure 10. Comparison of transverse stress plot for b/a = 0.1**

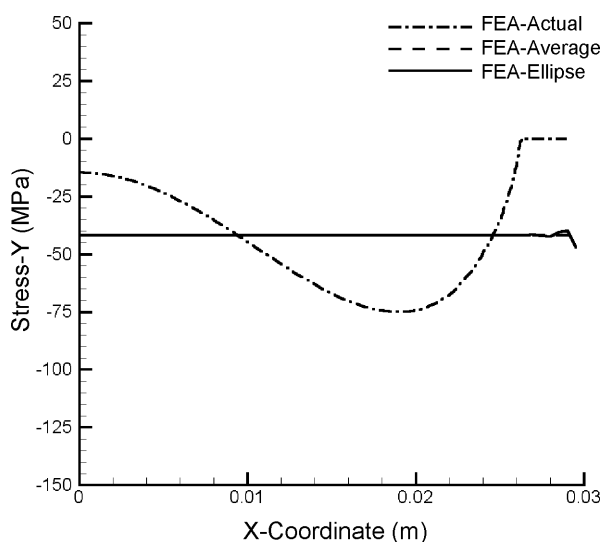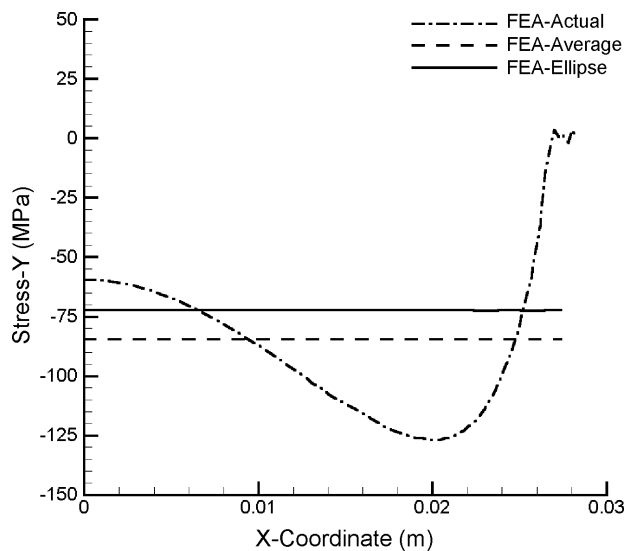**Figure 11. Comparison of transverse stress plot for b/a = 0.16**

Figure 12. Comparison of Transverse Stress Plot for b/a = 0.33

5.1 Calculation of Stress Intensity Factor for Transverse Isotropy

The stress intensity factor for the blunt elliptic inclusion case is calculated by using the Equation (14) for the formulation and compared with FEA results for a sharp crack. The numerical values are presented in **Table 3**. The stresses in Column 2 in **Table 3**, "Orthotropic Formulation", are the stresses for a blunt elliptic inclusion in a transversely isotropic matrix.

They are compared with the stresses in Column 3, "FEA Mean", which provides the mean value of the transverse stress along the major axis, included in **Figures 8** through **12**. **Figures 13 and 14** show the comparison graphically, with the compressive transverse stress σ_y in these graphs plotted without the negative sign. In general, good agreement is observed between the predicted transverse stresses. The maximum error in the predicted transverse stress is around 14% for the case of a crack with a thick

Table 3. Comparison of KI for transversely isotropic matrix with different a/b ratios

b/a	Stress σ_y (MPa)		Percentage Error	K_I (MPa $\sqrt{m}$)		Percentage Error
	Orthotropic Formulation	FEA Mean		Orthotropic Formulation	FEA	
0.033	-9.44	-9.09	3.85	2.90	2.58	12.40
0.066	-18.24	-18.61	1.99	5.60	5.12	9.38
0.10	-26.72	-26.70	0.08	8.20	7.54	8.75
0.166	-41.70	-41.70	0.00	12.79	12.52	2.16
0.333	-72.99	-84.60	13.72	22.39	23.14	3.24

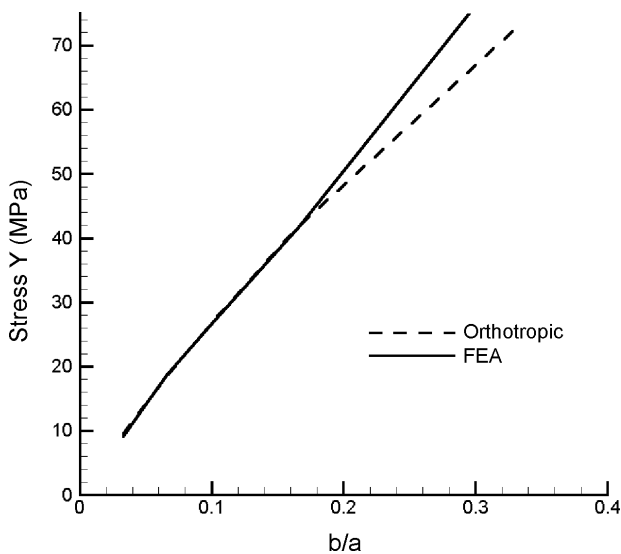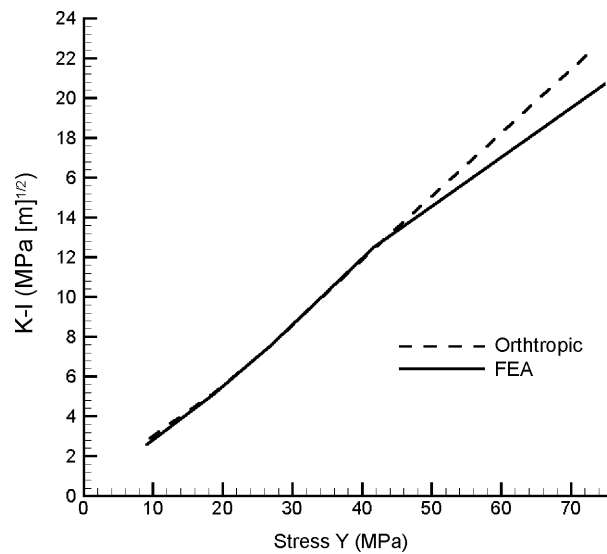**Figure 13. σ_y vs. b/a for Transversely Isotropic Matrix**

Figure 14. K_I vs. σ_y for Transversely Isotropic Matrix

inclusion, that is, b/a = 0.33. The maximum error in the predicted stress intensity is around 12%, but it occurs for the case of a crack with a thin inclusion, b/a = 0.033. It should be noted that the current formulation provides a conservative estimate for the stress intensity factor for most b/a ratios.

5.2 Benchmark Results for a Crack in an Orthotropic Lamina

For the case of an ice inclusion contained in a delamination between adjacent zero degree laminas within a unidirectional laminate, the matrix material will behave as a fully orthotropic material. For benchmarking of the orthotropic formulation with FEA results, the material properties given in Equation (4) and Equation (5) are used.

First, stresses and displacements resulting from the orthotropic formulation are compared with the

results obtained from FEA using orthotropic properties for the surrounding lamina. **Table 4** shows a comparison for the axial and transverse stresses for an elliptic inclusion, graphically illustrated in **Figures 15 and 16**. Similarly, the axial and transverse displacements along the inclusion boundary, for the case b/a = 0.16 (a/b = 6), are shown in **Figures 17 and 18**. It can be seen that the analytical results agree well with FEA predictions for axial stress, and the error in the transverse stress is about 17%.

6. ELLIPSE-CRACK EQUIVALENCE FOR AN ORTHOTROPIC MATRIX

As in the transversely isotropic case, the average value of the transverse stress over the length of the crack due to ice inclusion obtained from FEA is compared with results from FEA of the elliptic

Table 4. Comparison of stresses with FEA for blunt elliptic inclusion in a orthotropic matrix

b/a	Stress σ_x (MPa)		Percentage Error	Stress σ_y (MPa)		Percentage Error
	Orthotropic Formulation	FEA		Orthotropic Formulation	FEA	
0.033	-340.24	-344.90	1.35	-12.34	-14.85	16.90
0.066	-344.89	-350.82	1.69	-24.31	-29.16	16.63
0.10	-349.30	-356.24	1.95	-36.26	-42.96	16.00
0.166	-356.81	-365.68	2.43	-58.41	-69.05	15.41
0.333	-370.46	-382.29	3.09	-108.52	-126.17	13.99

Figure 15. Stress σ_x Comparison for Orthotropic Matrix
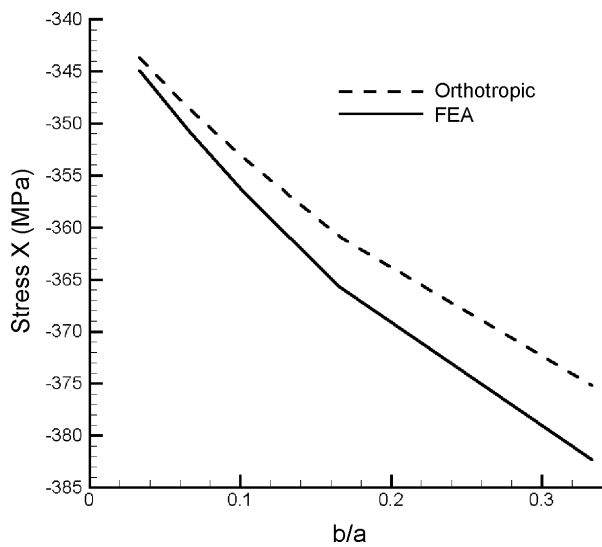

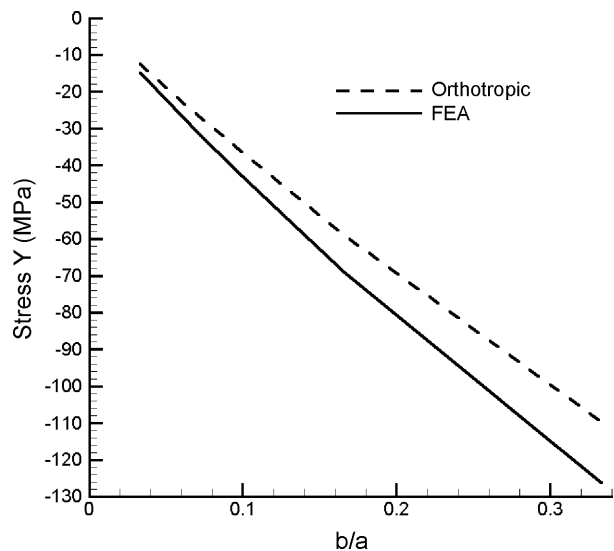**Figure 16. Stress σ_y Comparison for Orthotropic Matrix**

Figure 17. Comparison of X-Displacement for Orthotropic Matrix, b/a = 0.16
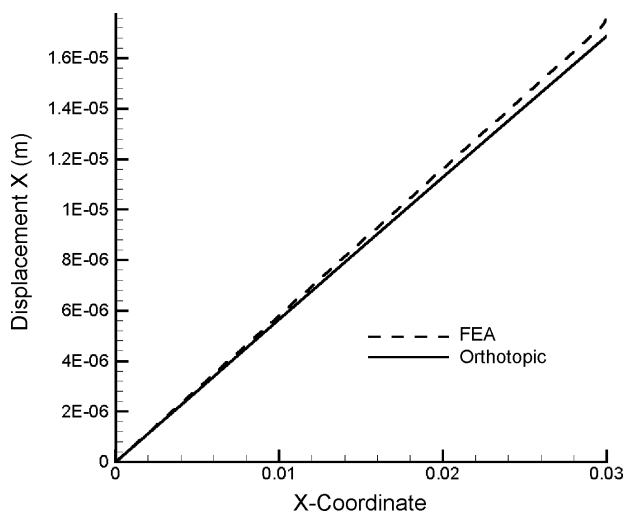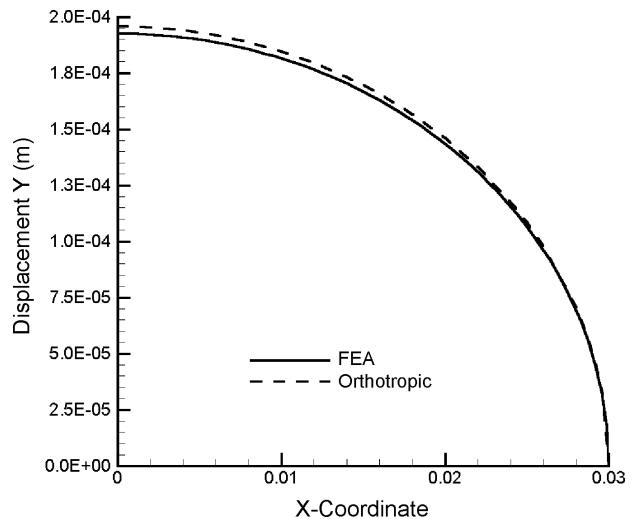

Figure 18. Comparison of Y-Displacement for Orthotropic Matrix, b/a = 0.16

inclusion in an orthotropic matrix. The variation of transverse stress σ_y along the semi-major axis for the crack(referred to as FEA-Actual), the average of σ_y for the crack (referred to as FEA-Average) and transverse stress along the semi-major axis of the equivalent ellipse (referred to as FEA-Ellipse) are plotted in **Figure 19** through **Figure 23**. It is seen that the average transverse stress in the crack and the transverse stress in the ellipse are in reasonably good agreement. These results are tabulated in **Table 5**.

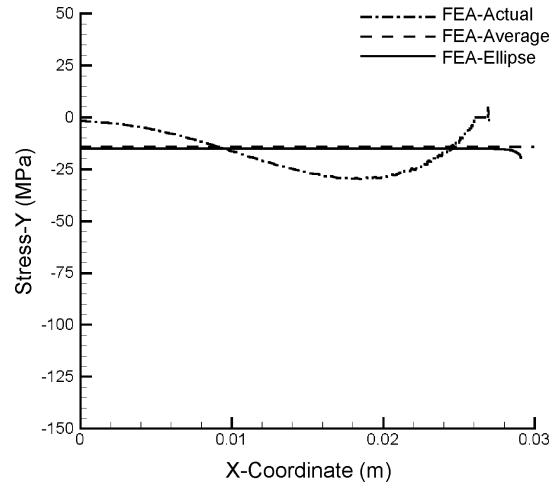**Figure 19. Comparison of Transverse Stress Plot for b/a = 0.033**

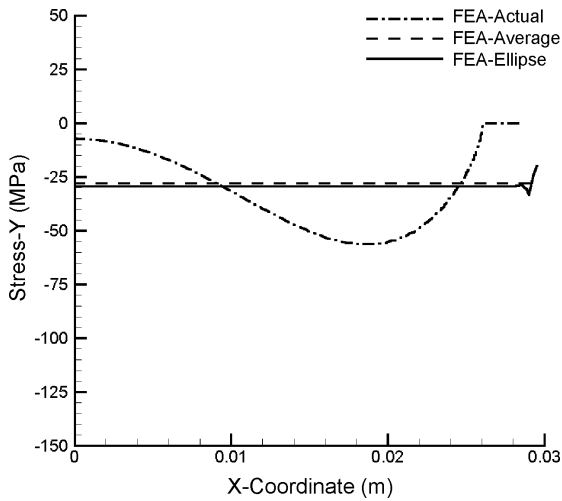**Figure 20. Comparison of Transverse Stress Plot for b/a = 0.066**

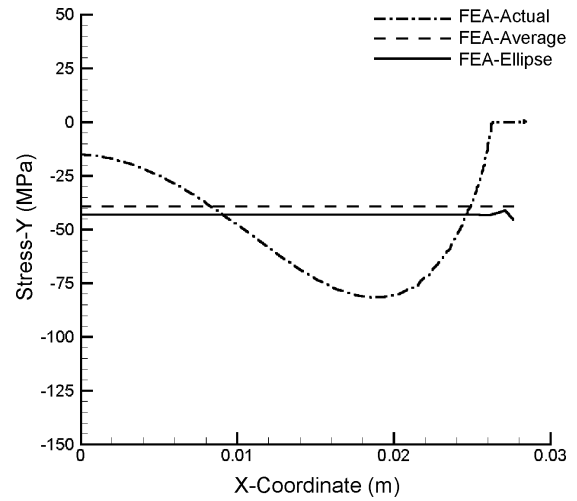**Figure 21. Comparison of Transverse Stress Plot for b/a = 0.1**

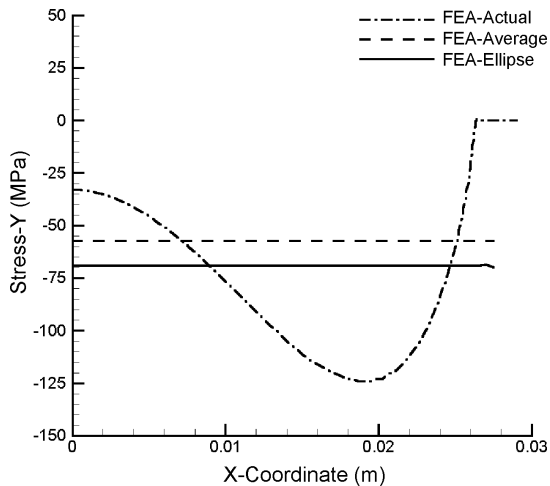**Figure 22. Comparison of Transverse Stress Plot for b/a = 0.16**

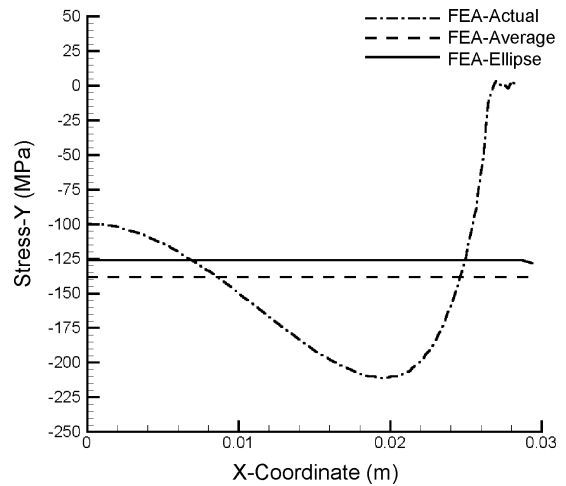**Figure 23. Comparison of Transverse Stress Plot for b/a = 0.33**

Table 5. Comparison of K_I for orthotropic matrix with different a/b ratios

b/a	Stress σ_y (MPa)		Percentage Error	K_I (MPa $\sqrt{m}$)		Percentage Error
	Orthotropic Formulation	FEA (Average)		Orthotropic Formulation	FEA (Average)	
0.033	-12.34	-14.1	12.48	3.79	3.74	1.34
0.066	-24.31	-27.9	12.87	7.46	7.38	1.08
0.10	-36.26	-39.2	7.50	11.13	10.88	2.30
0.166	-58.41	-59.3	1.50	17.93	17.89	0.22
0.333	-108.52	-138.0	21.36	33.31	34.34	3.00

7. STRESS INTENSITY FACTOR FOR ORTHOTROPIC MATRIX.

Results obtained for Mode I stress intensity factor, K_I, from the orthotropic formulation are tabulated in **Table 5** and are compared with FEA results for a crack with ice inclusion in an orthotropic lamina. The comparison with FEA results is also graphically depicted in **Figures 24 and 25**. The maximum error in the predicted stress intensity is only 3 % for the orthotropic case for a crack with a moderately slender ice inclusion, even though the corresponding error in the predicted transverse stress is 21 %. As in the case of the transversely isotropic lamina, it should be noted that the orthotropic formulation provides a conservative estimate for the stress intensity factor for most b/a ratios.

8. APPLICATIONS OF THE MODEL

Having benchmarked the proposed model using FEA results for ice-filled cracks in both transversely isotropic and orthotropic laminates, the model is now applied in a predictive mode to study certain interesting problems associated with the freezing of ice in a polymer composite laminate.

8.1 Ice Formation in Transverse Matrix Cracks

It is well known that cooling from cure temperature to room temperature or to sub-freezing temperatures results in residual stresses within a PMC laminate, because of difference of the elastic properties in adjacent plies. In order to study the detrimental effect of ice formation within micro cracks caused by residual
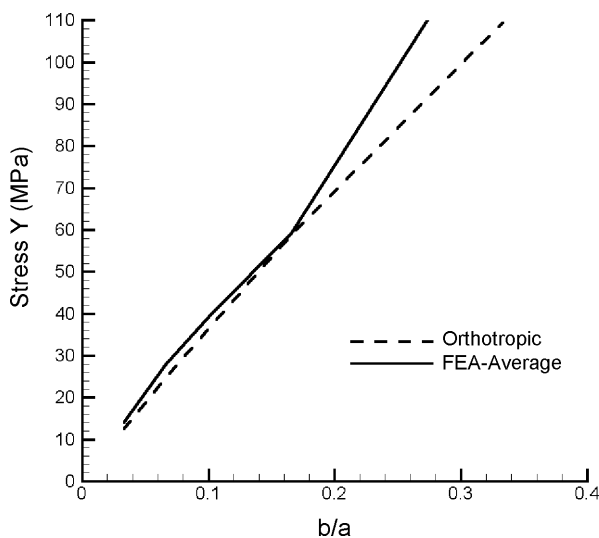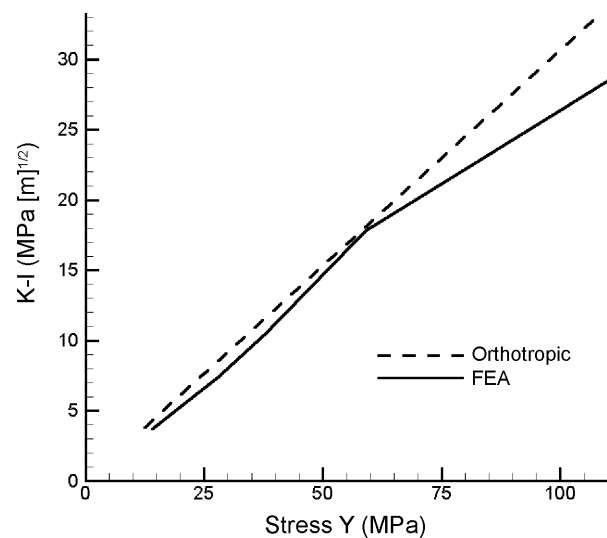
Figure 24. σ_y vs. b/a for Orthotropic Matrix

Figure 25. K_I vs. σ_y for Orthotropic Matrix

Samit Roy, G.H. Nie, R. Karedla and L. Dharani

stresses in a laminate, a $[0/90/0/90]_s$ T300/5208 graphite/epoxy laminate of total thickness 6.35 cm and the uniform thickness of each individual layer, h = 0.7935 cm is considered, as shown in **Figure 26**. A temperature change from 135 °C to 0 °C is applied to the laminate to simulate the temperature drop from cure to freezing. The longitudinal coefficient of thermal expansion (CTE) of the T300/5208 composite lamina is taken to be 0.02×10^{-6} m/°C and the thermal expansion coefficient in the transverse direction as 22.5×10^{-6} m/°C.

A single micro-crack is introduced in the [90/90] lamina at the center of the laminate as shown in **Figure 26** and, in the interest of tractability, interactions between multiple matrix cracks and delaminations is ignored. The length of the crack, 2a, is assumed to be 0.9 times the total thickness of [90/90] layers. In this context, Moschovidis et al[2] have shown that the interaction between two ellipsoidal inhomogeneities imbedded in an infinite matrix becomes negligible if the distance separating the inclusions is greater than four times the semi-major axis of the inclusions. Therefore, the predictions of the proposed analytical model would remain valid for matrix crack spacing greater than 4a, that is, for matrix crack densities less than L/4a. The longitudinal residual tensile stress present in the lamina would cause the micro-crack to open. Ignoring shearing tractions at the lamina interfaces, the crack opening

displacement (CTOD) for this case is given by Tada[11]:

$$CTOD = 2b = \frac{4\sigma a}{E'} V_1(a/h) \qquad (10)$$

where

$$V_1(a/h) = -0.071 - 0.535(a/h) + 0.169(a/h)^2$$
$$+0.02(a/h)^3 - 1.071\frac{1}{(a/h)}\ln(1-a/h) \qquad (11)$$

and h is the individual lamina thickness shown in **Figure 26**. For this case, from Equation (10), the semi-thickness of the ice inclusion $b = 8.477 \times 10^{-6}$ m, and the b/a ratio for the fully open micro-crack is therefore equal to 84.275.

It is envisioned that as the laminate cools down from its cure temperature, moisture diffuses into the open micro-crack. Finally, when the temperature reaches 0° C, the moisture freezes within the micro-crack. Assuming the material remains linear elastic and linear superposition is valid, the total stress intensity factor, K_I, at the crack tip consists of two additive components: (a) K_I due to the residual tensile stress in the matrix,

Figure 26. Ply lay-up for the $[0/90/0/90]_s$ T300/5208 graphite/epoxy laminate
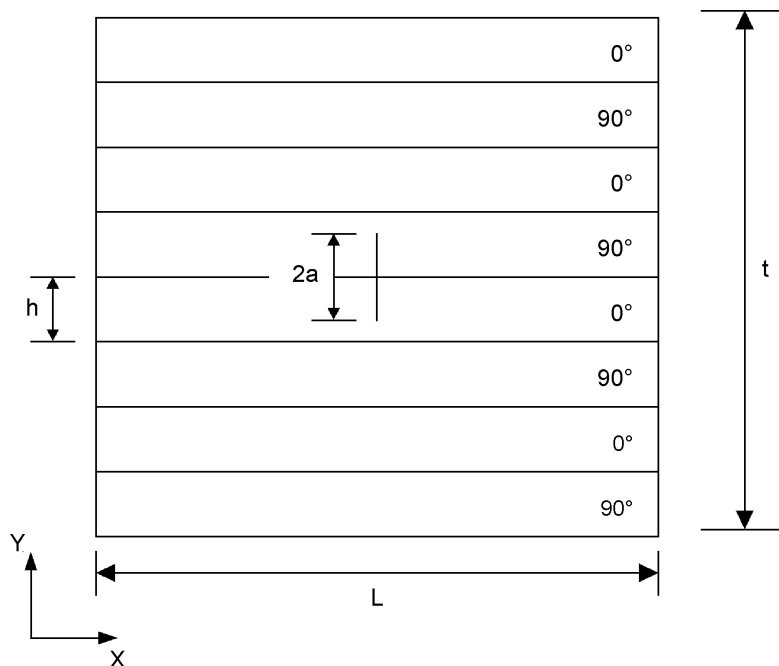
and (b) K_I due to the expansion of moisture in the micro-crack as it transforms to ice. The K_I due to freezing is calculated using the analytical formulation presented earlier. The K_I due to the residual stress in the matrix is calculated using results presented by Tada[11] for a finite width plate of thickness 2h containing a crack of length 2a,

$$K_I = \sigma \sqrt{\pi a} F(a/h) \qquad (12)$$

where,

$$F(a/h) = \frac{1 - 0.5(a/h) + 0.37(a/h)^2 - 0.044(a/h)^3}{\sqrt{1 - a/h}} \qquad (13)$$

The longitudinal residual tensile stress σ_1 in the 90° layers due to a cool down from 135°C to 0°C is obtained using a FORTRAN code based on classical lamination theory. The stress intensity factors obtained for this case are as given in **Table 6**. It can be seen that the increase in stress intensity due to ice formation in the micro-crack is only about 6% of the stress intensity due to residual stress for this case. However, it should be noted that the mitigating effect of swelling due to moisture absorption on residual tensile stress is not considered in this case.

Table 6. Comparison of stress intensity factors due to residual stress and inclusion stress

Type of Stress (MPa)	Magnitude of Stress (MPa)	K_I (MPa √m)
Residual Thermal Stress	28.71	3.51
Inclusion Stress due to Ice Formation	4.48	0.212

From **Table 6**, it can be observed that the increase in stress intensity due to the presence of ice inclusion is approximately 6% of the stress intensity due to residual thermal stresses in the lamina at 0 °C. It can therefore be concluded that for the material system considered and the assumed temperature drop, the contribution of ice formation in the micro-cracks to the overall stress intensity and to laminate failure initiation is not very significant.

8.2 Analysis of Delamination in a Laminate Due to Ice Formation

8.2.1 Local Versus Global Modeling Issues

The orthotropic formulation is employed to predict the effect of ice formation within a delamination along the laminate mid-plane as shown in **Figure 27**.

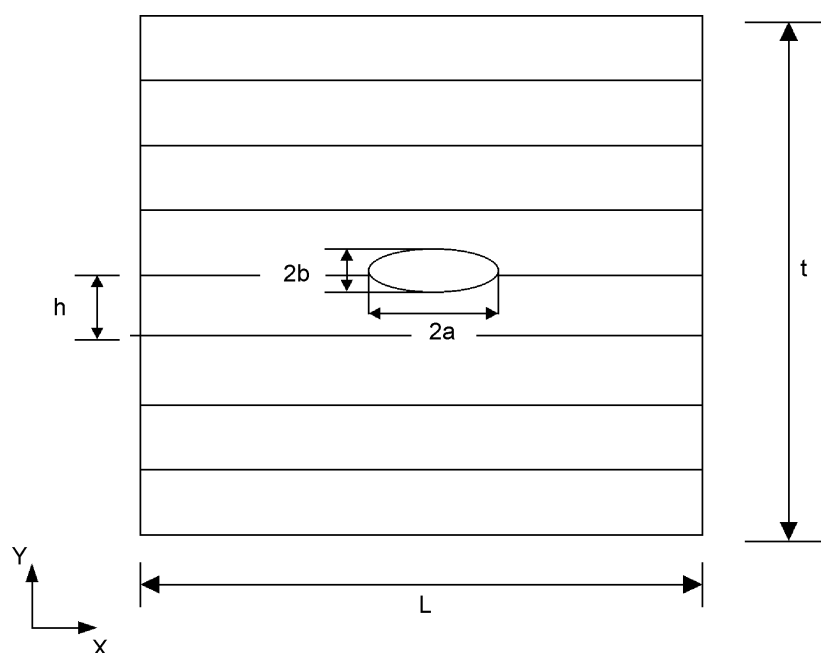**Figure 27. Mid-Plane Delamination in a Laminate**

Samit Roy, G.H. Nie, R. Karedla and L. Dharani

Table 7. Local vs. global effect in stress intensity factor for delamination					
Laminate	K_I (MPa ÷m)		Percentage Error	K_I (MPa √m)		Percentage Error
	Local Ply Properties	FEA		CLT	FEA	
$[0/90/0/90]_s$	3.24	3.08	5.08	8.35	3.08	171.1
$[90/0/90/0]_s$	4.56	4.62	1.42	8.35	4.62	80.73

Because delamination is governed by local stress fields in the vicinity of the crack tip, it is anticipated that only local ply material properties, that is, material properties of the plies adjacent to the delamination, need to be input to the analytical model. However, in order to ascertain if the crack driving force at the tip of the delamination is in anyway influenced by the overall laminate stiffness, stress intensity factors for the following cases are evaluated using the analytical model and compared with FEA results: (a) delamination between the adjacent [90/90] laminas in a $[0/90/0/90]_s$ laminate and (b) delamination between the [0/0] laminas in a $[90/0/90/0]_s$ laminate. In each case, the analytical model predictions for K_I are obtained using local ply properties, (**Table 7**, Column 1), followed by analytical model predictions for K_I using global laminate properties obtained using classical lamination theory (CLT) (**Table 7**, Column 4).

To benchmark these results with FEA, a quarter symmetry model of a t = 12.7 mm thick and L = 25 mm wide laminate is constructed. Each lamina is modeled for a thickness of h = 1.5875 mm. The semi major axis, a, of crack is modeled as 1.905 mm and the semi minor axis, b, is modeled as 0.3175 mm to give b/a = 0.166. The results shown in **Table 7** indicate that the stress intensity factor is governed primarily by the local material properties, and that using the equivalent stiffness calculated using CLT, could lead to erroneous results. As can be seen from the first two columns in **Table 7**, for both $[0/90/0/90]_s$ and $[90/0/90/0]_s$ laminates, the stress intensity factor depends strongly on the properties of the adjacent lamina. Thus, for delamination between the [90/90] lamina in a [0/90/0/90]s laminate, transversely isotropic properties of the [90] lamina are input into the orthotropic formulation. Similarly, for delamination between the [0/0] lamina of $[90/0/90/0]_s$, laminate orthotropic material properties for the [0] lamina are input into the formulation. The stress intensity factor predicted by the model with equivalent global stiffness calculated using CLT are much higher than the FEA results, thereby vindicating the local approach.

8.2.2 Delamination Analysis

In general, two types of delamination are possible in laminates, i.e., (1) Free Edge Delamination and (2) Local or Transverse Crack Tip Delamination. The free edge delamination is a result of stresses at the free edge of the laminate. Transverse crack tip delamination occurs when a transverse crack as shown in **Figure 26** impinges on the interface between two lamina, which often results in the delamination of the laminate. Crack initiation due to trapped water freezing in a local (Type 2) delamination is studied, as shown in **Figure 27**. The orthotropic formulation is employed for a $[0/90/0/90]_s$ laminate for different cases of delamination opening displacement, i.e., b/a ratios. For each case, self similar delamination growth, i.e., b/a is assumed to remain constant. The delamination length, a, is increased to obtain the critical delamination length that would correspond to the critical energy release rate, G_{IC}, for each selected value of b/a. The dimensions of the individual lamina and laminate are as shown in **Figure 27**. The G_{IC} for the material is assumed to be 125 J/m², based on results presented by Armanios et al[12]. **Figure 28** shows the variation of crack driving force due to increase in delamination length for each b/a ratio.

The equation of each b/a=constant curve is given by

$$G = J = \frac{K_I^2}{E'} = \frac{\pi \sigma_y^2 a}{E'} \tag{14}$$

In Equation (14) σ_y is a constant, as it is only a function of b/a (derived by substituting Equation (35) in Equation (9) in Roy et al[1]), and are also constants resulting in the crack driving force, G, to be a linear function of delamination length, a. Therefore, as shown in **Figure 28**, the curve for a given value of ratio, b/a, is a straight line with a slope equal to

$$S = \frac{\pi \sigma_y^2}{E'} \tag{15}$$

Figure 28. Delamination Driving Force vs. Delamination Length
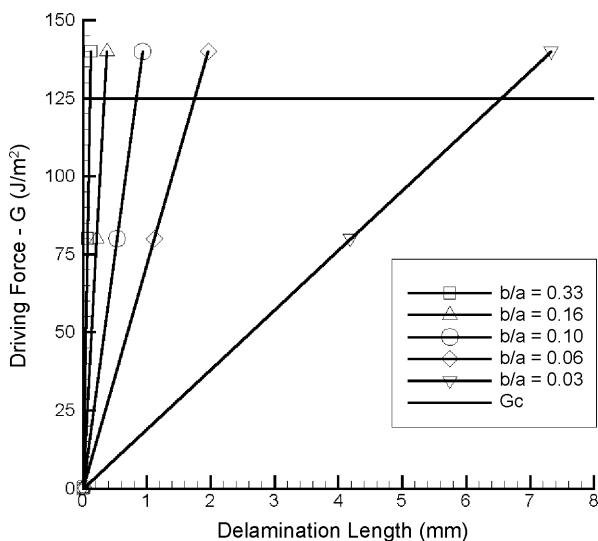
and passing through the origin as indicated by equation (14). It should be noted that though σ_y is a constant for any given value of ratio b/a, its magnitudes will be different for different values of ratio b/a, which accounts for the different slopes of the curves in **Figure 28**. **Table 8** give the critical delamination length, a_c, which corresponds to the point of intersection of the b/a curves and the critical strain energy release rate (G_c) line in **Figure 28**, assuming no increase in resistance with delamination growth. It is also interesting to note that as the orthotropic formulation is independent of the dimensions of the matrix, and is only dependent of the inclusion dimensions (a and b), the critical values of delamination presented in **Table 8** are valid for any dimension of the matrix for the material chosen, as long as there are no edge effects and adjacent delaminations influencing the stress field in the inclusion

Table 8 Critical delamination lengths for frost delamination	
b/a	Critical Delamination Length, a_c (mm)
0.03	6.54
0.06	1.75
0.10	0.83
0.16	0.34
0.33	0.11

8.2.3 Life Prediction for Freeze-Thaw Cycling

As a demonstration of the predictive methodology, a freeze-thaw delamination growth analysis is performed on a $[0/90/0/90]_s$ laminate depicted in **Figure 27** and with material properties as given in section 8.2.2. The following equations based on Paris law are used to calculate the number of freeze-thaw cycles, which result in complete delamination between the [90/90] laminas.

The prediction on fatigue life can be performed by using Paris law expressed below

$$N_f = \int_{a_i}^{a_f} \frac{da}{C(K_I)^m} \qquad (16)$$

The law has an equivalent form where K_I is replaced by the strain energy release rate G as follows,

$$N_f = \int_{a_i}^{a_f} \frac{da}{C(G)^m} \qquad (17)$$

where, the material constants C, m are not the same as that in equation (16). As a demonstration of the predictive methodology, a freeze-thaw delamination growth analysis is performed on a $[0/90/0/90]_s$ laminate depicted in **Figure 27** and with material properties as given in section 8.2.2. The equation (17) is used to determine the number of freeze-thaw cycles, which result in complete delamination between the [90/90] laminas. The number of cycles is calculated for a crack growth from 1.5875 mm (i.e., initial delamination length equal to single lamina thickness) to 25 mm (i.e., assumed length of the laminate). For evaluation of the integral in Equation (17), the crack growth is assumed to be self-similar, i.e. b/a ratio remains constant with time during the freeze-thaw cycles. The constant b/a ratio is taken to be equal to 0.16 for this study, simulating a relatively slender inclusion. The fatigue crack growth material parameters employed in this analysis are based on results presented by Prel et al[13],

$$m = 10.5$$

$$C = 3.1 \times 10^{-40} \frac{mm}{cycles\,(J/m^2)^{10.5}} \qquad (18)$$

Substituting equation (14) in (17) gives,

$$N_f = \int_0^{N_f} dN = \int_{a_0}^{a_f} \frac{da}{C\left(\pi\sigma_y^2 a / E'\right)^m} \tag{19}$$

After substituting for σ_y, C and m for the selected material system and integrating Equation (19), the resulting fatigue-life parameters are tabulated in **Table 9**. As can be seen, 4.8923×10^9 freeze-thaw cycles are predicted for this case to completely delaminate the composite. However, the simple predictive model does not account for edge effects and potential interaction with other damage states when the delamination approaches the free edges of the laminate.

Table 9. Freeze-thaw cycle parameters

b/a	0.16
a_i	1.5875 mm
a_f	25 mm
N_f	4.8923×10^9 cycles

For the case that the delamination growth is not self-similar, i.e., when the ratio b/a is not a constant, the integral in Equation (19) can still be evaluated using numerical integration method, such as, Gaussian quadrature.

9. SUMMARY AND CONCLUSIONS

An analytical formulation to calculate the stress intensity factor K_I due to water-ice inclusion in both transversely isotropic and orthotropic matrices was successfully developed and verified. With the help of FEA, it was established that stress field in the vicinity of an elliptic inclusion was an acceptable analytical idealization to obtain the stress intensity for a crack with ice inclusion. In this context, it has been shown that the interaction between two ellipsoidal inhomogeneities imbedded in an infinite matrix becomes negligible if the distance separating the inclusions is greater than four times the semi-major axis of the inclusions. Therefore, the predictions of the proposed analytical model would remain valid for crack spacing greater than 4a, that is, for matrix crack densities less than L/4a. It was observed that for the case of an inclusion with a sharp tip, the transverse stress distribution was in the shape of a cosine curve with its mean value close to the transverse stress predicted for a blunt-tip elliptic inclusion having the same b/a ratio. Stress intensity factor, K_I, obtained for various values of a/b are in reasonable agreement with the corresponding results from FEA analysis. Though the model under-predicts the stress intensity factor for moderately thick ellipse, the stress intensity factors obtained for slender ellipses were conservative. For the material system used, the model predicted near exact stress intensity factor for b/a = 0.1666. A simple methodology to predict static delamination failure and the fatigue durability of a cross-ply laminate subject to freeze-thaw cycling was demonstrated. Even though the analytical model was benchmarked using FEA results, experimental verifications of the analytical predictions are necessary to rigorously validate the analytical derivation.

REFERENCES

1. Roy, S., Nie, G.H., Karedla, R. and Dharani, L., Matrix cracking and delaminations in orthotropic laminates subjected to freeze-thaw: Model Development, Polymers and Polymer Composites, 2002, 10: 327-339.

2. Moschovidis, ZA and Mura, T., Two-ellipsoidal inhomogeneities by the equivalent inclusion method. ASME J. Applied Mech., December 1975, 42:847-852.

3. Li, H., Zhong, W.F. and Li, G.F., Equivalent inclusion method in elastodynamics and the scattered field for two-ellipsoidal inhomogeneities, Appl. Math. Mech., 1985, 6: 489-498.

4. Zhong, W.F. and Nie, G.H., An Integral Equation of the Scattering Problem by Many Inhomogeneities and the Scattered Effect, Applied Mechanics, vol.2, 1989, 1003-1008.

5. Zhong, W.F. and Nie, G.H., The Scattering of SH Waves by Numerous Inhomogeneities in an Anisotropic Body, Acta Mechanica Solida Sinica, 1988, 1: 81-96.

6. Wang, J. and Karihaloo, B.L., Matrix-crack induced delamination in composite laminates under transverse loading. Composite Structures, 1997, 38:661-6.

7. Christensen, R.M., A critical evaluation for a class of micro-mechanics models, J Mech. Phys. Solids, 1990, 38:379-404.

8. Nemat-Nasser, S. and Hori M., *Micromechanics: Overall Properties of Heterogeneous Materials*, North-Holland, 1993.

9. Kanninen, M. F. and Popelar, C. H., Advanced Fracture Mechanics. Oxford University Press, (1985).

10. Bhargava, R. D. and Radhakrishna, H. C., Two-dimensional elliptic inclusions. Proc. Camb. Phil. Soc., 59, (1963), p. 811.

11. Tada, H., Paris, P. C. and Irwin, G., R., Stress analysis of cracks handbook. Del Research Corporation, (1973).

12. Armanios, E. A., Sriram, P. and Badir, A. M., Fracture Analysis of Transverse Crack-Tip and Free-Edge Delamination in Laminated Composites. Composite Materials: Fatigue and Fracture, ASTM STP 1110, (1991).

13. Prel, J., Davies, P. and Benzeggagh, M. L., Mode I and Mode II Delamination of Thermosetting and Thermoplastic Composites. Composite Material: Fatigue and Fracture, ASTM STP 1012, (1989).

ACKNOWLEDGEMENT